NASA TECHNICAL MEMORANDUM

NASA TM X-2941

NASA TM X-2941

EXPERIMENTAL INVESTIGATION AT MACH 8 OF THE EFFECTS OF PROJECTIONS AND CAVITIES ON HEAT TRANSFER TO A MODEL OF THE VIKING AEROSHELL

by Theodore R. Creel, Jr.

Langley Research Center
Hampton, Va. 23665

NATIONAL AERONAUTICS AND SPACE ADMINISTRATION • WASHINGTON, D. C. • APRIL 1974

1. Report No.	2. Government Accession No.	3. Recipient's Catalog No.
NASA TM X-2941		

4. Title and Subtitle	5. Report Date
EXPERIMENTAL INVESTIGATION AT MACH 8 OF THE EFFECTS OF PROJECTIONS AND CAVITIES ON HEAT TRANSFER TO A MODEL OF THE VIKING AEROSHELL	April 1974
	6. Performing Organization Code
7. Author(s)	8. Performing Organization Report No.
Theodore R. Creel, Jr.	L-9244
9. Performing Organization Name and Address	10. Work Unit No.
NASA Langley Research Center Hampton, Va. 23665	815-20-09-08-02
	11. Contract or Grant No.
12. Sponsoring Agency Name and Address	13. Type of Report and Period Covered
National Aeronautics and Space Administration Washington, D.C. 20546	Technical Memorandum
	14. Sponsoring Agency Code

15. Supplementary Notes

16. Abstract

An experimental investigation into the aerodynamic heating on a Mars entry vehicle shape with several types of local surface distortion is presented. The configurations tested were 0.033-scale models of a spherically blunted 70° half-angle cone with two protuberances of different length, representing the tube leading to the gas chromograph mass spectrometer, and two aeroshell-bioshield attachment points of different size. These models were tested at free-stream Reynolds numbers per meter of 3.7×10^6 and 17×10^6 over an angle-of-attack range from 0° to 18° in the Langley Mach 8 variable-density hypersonic tunnel. The phase-change-coating technique was used to measure heat-transfer coefficient.

The long protuberance caused more severe interference heating than the short protuberance for the same conditions. When the short projection was located close to the edge of the aeroshell, the interference heating was greater than that on the same projection when located near the vertex. A significant increase in heat-transfer coefficient was measured only on the larger aeroshell-bioshield attachment point.

17. Key Words (Suggested by Author(s))	18. Distribution Statement
Heat transfer Convective heating Aerodynamic heating	Unclassified – Unlimited STAR Category 33

19. Security Classif. (of this report)	20. Security Classif. (of this page)	21. No. of Pages	22. Price*
Unclassified	Unclassified	53	$3.75

*For sale by the National Technical Information Service, Springfield, Virginia 22151

EXPERIMENTAL INVESTIGATION AT MACH 8 OF THE EFFECTS OF PROJECTIONS AND CAVITIES ON HEAT TRANSFER TO A MODEL OF THE VIKING AEROSHELL

By Theodore R. Creel, Jr.
Langley Research Center

SUMMARY

An experimental investigation into the aerodynamic heating on a Mars entry vehicle shape with several types of local surface distortion is presented. The configurations tested were 0.033-scale models of a spherically blunted 70° half-angle cone with two protuberances of different length, representing the tube leading to the gas chromograph mass spectrometer, and two aeroshell-bioshield attachment points of different size. These models were tested at free-stream Reynolds numbers per meter of 3.7×10^6 and 17×10^6 over an angle-of-attack range from 0° to 18° in the Langley Mach 8 variable-density hypersonic tunnel. The phase-change-coating technique was used to measure heat-transfer coefficient.

The long protuberance caused more severe interference heating than the short protuberance for the same conditions. When the short projection was located close to the edge of the aeroshell, the interference heating was greater than that on the same projection when located near the vertex. A significant increase in heat-transfer coefficient was measured only on the larger aeroshell-bioshield attachment point.

INTRODUCTION

An unmanned Mars lander mission will be accomplished in 1976 to investigate several important aspects of the atmospheric and surface conditions of Mars, with the most important goal being the determination of life (in any form) on that planet. (See ref. 1.) As stated in the reference, this investigation will be performed under the most trying conditions even after the planet has been reached by the spacecraft. Thus, before the spacecraft has left the Earth's surface, every imaginable effort will have been made to insure the complete success of this mission. For example, the shape of the spacecraft was chosen only after the structural integrity and payload capability of various configurations had been studied (ref. 2). Also, many experimental and theoretical studies of the aerodynamic characteristics of different configurations were completed. (See refs. 3, 4, 5, and 6.)

Aerodynamic heat-transfer characteristics of the final configuration, a spherically blunted 70° half-angle cone, were reported in reference 7, but this study neither considered the aerodynamic heating on a projection (tube leading to the gas chromograph mass spectrometer) nor investigated the aerodynamic heating of the aeroshell-bioshield attachment points which are three cavities located 120° apart on the aeroshell. The purpose of this report is to present the results of an investigation into the aerodynamic heating of five (0.033 scale) configurations of the Mars entry vehicle (as of June 8, 1971). These models were tested over an angle-of-attack range from 0° to 18° at free-stream Reynolds numbers per meter of 3.7×10^6 and 17×10^6 in the Langley Mach 8 variable-density hypersonic tunnel.

SYMBOLS

c	specific heat of model material, J/kg-K
H	local heat-transfer coefficient, W/m^2-K
H_S	reference stagnation-point heat-transfer coefficient, W/m^2-K; HS in computer plots
k	thermal conductivity of model material, W/m-K
L	length of projection, cm (see fig. 1)
R	free-stream Reynolds number per meter (based on maximum model diameter); R/M in computer plots
r_b	maximum model radius, cm
s	surface distance measured on model from nose vortex, cm
t	time, sec; T in computer plots
α	angle of attack, deg
ρ	density of model material, kg/m^3
ϕ	radial angle, deg

APPARATUS AND TESTS

Facility

The facility used in this test program was the Langley Mach 8 variable-density hypersonic tunnel described in reference 8. To obtain in air a Reynolds number range from 3.7×10^6 to 17×10^6, the stagnation pressure was varied from 1.38 to 7.93 MN/m^2 with stagnation temperature ranging from 672 K to 783 K. The tunnel has a contoured axisymmetric nozzle with a test-section diameter of 45.7 cm and a model injection mechanism located directly beneath the test section.

Models

The models were made of a high-temperature plastic so that during the heat-transfer phase of the tests heat-transfer rates could be obtained by using fusible temperature indicators (ref. 9). Model 1 (fig. 1) is the basic shape of the Mars entry aeroshell configuration with a 0.033-scale spherically blunted 70^o half-angle cone; the afterbody is not to scale. Models 2 to 5 consist of the basic shape, projections representing the mass spectrograph probe, and cavities representing the aeroshell-bioshield attachment points. Model 2 has a long protuberance (0.818 cm long, 0.1626 cm in diam.) to simulate the mass spectrograph probe and the aeroshell-bioshield attachment points A shown in figure 2. Model 3 differs from model 2 in that it has a short projection (0.0864 cm long, 0.1626 cm in diam.) to represent the mass spectrograph probe and the aeroshell-bioshield attachment points A shown in figure 2. Model 4 is simply model 3 rotated and positioned at an angle of attack so that one aeroshell-bioshield attachment point is located on the most windward ray. Model 5 is shown in figure 3 and differs from the previous models by having the projection (0.0864 cm long, 0.1626 cm in diam.) representing the mass spectrograph probe located near the edge of the cone and having the aeroshell-bioshield attachment points B shown in figure 2.

Test Technique

The fusible-temperature-indicator technique described in reference 9 was used to determine heat-transfer coefficients. Briefly, a thin layer of contrasting color pigment of known melting temperature is sprayed on the model outside the wind tunnel. When the tunnel flow has been established, the model is injected into the flow and two motion-picture cameras photograph the model at known time intervals. The assumption of one-dimensional heat flow inside the model permits the calculation of an aerodynamic heat-transfer rate (ref. 9) by relating the time to reach the melting temperature and the model thermal properties. For the present tests, the adiabatic wall temperature was calculated by assuming a laminar recovery factor of 1.0 and a Newtonian pressure distribution.

(For these very low Mach numbers on the face of the model, the ratio of adiabatic wall temperature to free-stream total temperature was always above 0.99; thus, the effect of recovery factor is essentially negligible.) The computed heat-transfer coefficients were then normalized by the value calculated (by using ref. 10) for the stagnation point on a sphere having a radius of 2.921 cm (equal to the aeroshell nose radius).

To simplify locating the isothermal lines on the models, each set of figures in which phase-change patterns are shown contains a grid model. For the present tests two different grid models were used. Grid model 1 was divided into 14 equal angles even though these angles may not be seen in the figures. The values of the ratio of the surface distance s of each concentric circle to the base radius r_b of grid model 1 are presented in table I. Grid model 2 was divided into 12 equal angles, and the surface locations of the concentric circles are shown in table II. The most windward ray is at $\phi = 0^o$.

The model thermal properties $\left(\sqrt{\rho ck}\right)$ were obtained by testing samples of the same material used in the model construction. Each value of ρ, c, and k used was an average of three individual tests. The $\sqrt{\rho ck}$ values used are as follows:

Model	$\sqrt{\rho ck}$
1	0.08166
2	.07804
3,4	.07672
5	.079

The $\sqrt{\rho ck}$ value for model 5 is the average of the $\sqrt{\rho ck}$ values for models 1, 2, and 3.

RESULTS AND DISCUSSION

Tests were made in the Langley Mach 8 variable-density hypersonic tunnel to obtain the heat-transfer coefficients on five different configurations of a Mars entry vehicle. The tests were conducted at angles of attack from 0^o to 18^o over a Reynolds number range from 3.7×10^6 to 17×10^6. The results of these tests are presented in figures 4 to 16. These figures include a graphic representation of the grid model used to locate isotherms on the models. Also included in each figure beneath the appropriate model is the Reynolds number per meter, the isotherm number, the calculated reference stagnation-point heat-transfer coefficient, and the ratio of the measured heat-transfer coefficient for each contour to the theoretical stagnation-point heat-transfer coefficient. Some duplication of tests is shown in these figures, which was thought to be needed in order to better define the heating at certain locations on the body. Also, during each test two cameras (one 90^o to the other) photographed the model; thus, two views are shown for some of the tests.

The heat-transfer coefficients are plotted as a function of s/r_b in figures 17 to 19. The heat-transfer data for the windward ray of the aeroshell at angles of attack of 3^o, 9^o, and 18^o are compared for models 1, 2, and 3 in figure 17 at a Reynolds number per meter of 3.7×10^6 and in figure 18 for a Reynolds number per meter of 17×10^6. As angle of attack is increased from 3^o to 18^o, the heat transfer to the basic model (fig. 17(a)) shows an increase of approximately 20 percent. The curves drawn in figures 17(a), 18(a), and 19 are only to indicate trends and should not be considered an accurate estimate of local values between points. Figure 17(b) presents the heat-transfer data of model 2, which has the long projection, at $\alpha = 3^o$ and 9^o and Reynolds number per meter of 3.7×10^6 and compares these data with those of model 1 (fig. 17(a)). An increase in heat transfer of about 20 percent is evident near the projection for an angle of attack of 9^o. The heat-transfer coefficients of model 3, which has the short projection, show a 30-percent increase when compared with those of model 1, but this increase occurs only at an angle of attack of 18^o. (See fig. 17(c).)

Figure 18 presents the windward-ray heating on models 1, 2, and 3 at a Reynolds number per meter of 17×10^6 for angles of attack of 3^o, 9^o, and 18^o. At this Reynolds number, the heat-transfer coefficients of model 1 increased approximately 30 percent as the angle of attack increased from 3^o to 18^o (fig. 18(a)). Model 2 (fig. 18(b)) experienced an increase of approximately 40 percent over the basic model for the same Reynolds number and angle-of-attack range. Apparently the thin boundary layer associated with the higher Reynolds number makes interference from the long projection more pronounced.

The aerodynamic heating on the windward ray of model 5 is presented in figure 19 for an angle-of-attack range from 0^o to 18^o at Reynolds numbers of 3.7×10^6 and 17×10^6. The principal effect of increasing the Reynolds number from 3.7×10^6 to 17×10^6 (figs. 19(a) and 19(b), respectively) is to increase the measured heat-transfer-coefficient ratios H/H_S in the projection area to values as high as 2.2 to 2.5. In general, the effect of the projections is to increase local heating downstream of the projection as well as in the immediate vicinity.

The aeroshell-bioshield attachment points B were machined on model 5 with the intent of determining the difference in heating on attachment points A and B. Since heat-transfer coefficients were not obtained (for the same conditions) on attachment point B of figure 2, a numerical ratio of the heat-transfer coefficients on the two different aeroshell-bioshield attachment points cannot be given (A being larger than B). However, the results indicate that attachment point A will have more interference heating than attachment point B.

The schlieren photographs of figure 20 are typical of those of this investigation and do not show any local perturbations of the shock wave.

CONCLUSIONS

An experimental investigation to determine the effects of projections and cavities on the heating on five models of the Mars entry configuration was conducted in the Langley Mach 8 variable-density hypersonic tunnel at free-stream Reynolds numbers per meter of 3.7×10^6 to 17×10^6 over an angle-of-attack range from 0° to 18°. The conclusions drawn from this investigation are as follows:

1. For projections near the vertex of the nose, the long projection apparently caused larger heat-transfer coefficients in its immediate area than did the short projection.

2. The projection located near the edge of the aeroshell produced higher heating rates than the same size projection near the vertex (approximately 2.5 times the calculated stagnation-point-heat-transfer coefficient).

3. The larger aeroshell-bioshield attachment points produced significant heat-transfer increases above those of the basic model, but the heating around the smaller attachment points was approximately equal to the heating on the basic model.

Langley Research Center,
National Aeronautics and Space Administration,
Hampton, Va., February 5, 1974.

REFERENCES

1. Soffen, Gerald A.; and Martin, James S., Jr.: How We'll Search for Life on Mars. Popular Science Monthly, vol. 198, no. 2, Feb. 1971, pp. 51-53, 134, 136.

2. Guy, L. D.: Structural and Decelerator Design Options for Mars Entry. J. Spacecraft & Rockets, vol. 6, no. 1, Jan. 1969, pp. 44-49.

3. Sawyer, James Wayne: Comparison of the Mach 3.0 Aerodynamic Characteristics of Tension String, Tension Shell, and 120° Conical Shapes. NASA TN D-4360, 1968.

4. Bernot, Peter T.: Longitudinal Stability Characteristics of Several Proposed Planetary Entry Vehicles at Mach 6.73. NASA TN D-2785, 1965.

5. Robinson, James C.; and Jordan, Alfred W.: Exploratory Experimental Aerodynamic Investigation of Tension Shell Shapes at Mach 7. NASA TN D-2994, 1965.

6. McGhee, Robert J.; Siemers, Paul M., III; and Pelc, Richard E.: Transonic Aerodynamic Characteristics of the Viking Entry and Lander Configurations. NASA TM X-2354, 1971.

7. Faye-Petersen, R.; Sarver, D.; and Carroll, H.: Heat Transfer and Pressure Distributions at $M = 8$ on 0.029 Scale Models of the Viking Entry Vehicle. TP-3720318 (Contract NAS1-9000), Martin Marietta Corp., July 1972.

8. Stainback, P. Calvin: Heat-Transfer Measurements at a Mach Number of 8 in the Vicinity of a 90° Interior Corner Alined With the Free-Stream Velocity. NASA TN D-2417, 1964.

9. Jones, Robert A.; and Hunt, James L.: Use of Fusible Temperature Indicators for Obtaining Quantitative Aerodynamic Heat-Transfer Data. NASA TR R-230, 1966.

10. Reshotko, Eli; and Cohen, Clarence B.: Heat Transfer at the Forward Stagnation Point of Blunt Bodies. NACA TN 3513, 1955.

TABLE I.- COORDINATES OF GRID MODEL 1

Coordinate location	s/r_b
Grid 1	0.110
Grid 2	.204
Grid 3	.313
Grid 4	.421
Grid 5	.508
Grid 6	.617
Grid 7	.726
Grid 8	.813
Grid 9	.900
Grid 10	.987
Aeroshell edge	1.048
Projection	.076
Sphere-cone junction	.175
Aeroshell-bioshield attachment point	.456

TABLE II.- COORDINATES OF GRID MODEL 2

Coordinate location	s/r_b
Grid 1	0.104
Grid 2	.222
Grid 3	.330
Grid 4	.446
Grid 5	.554
Grid 6	.672
Grid 7	.787
Grid 8	.898
Grid 9	1.017
Aeroshell edge	1.048
Projection	.895
Sphere-cone junction	.175
Aeroshell-bioshield attachment point	.456

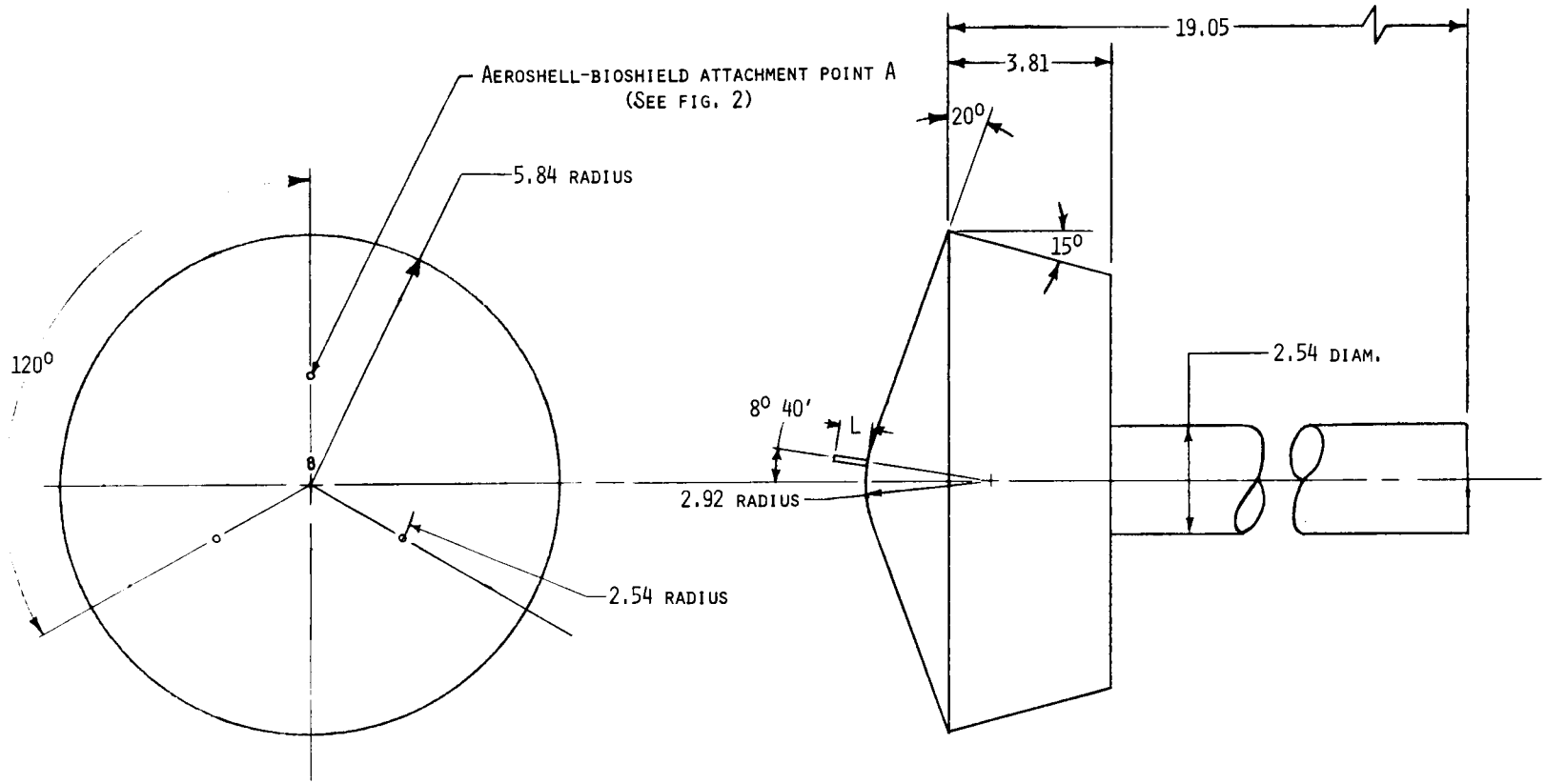

Figure 1.- Schematic of basic Mars entry configuration (model 1) showing projections and cavities. All linear dimensions are in centimeters.

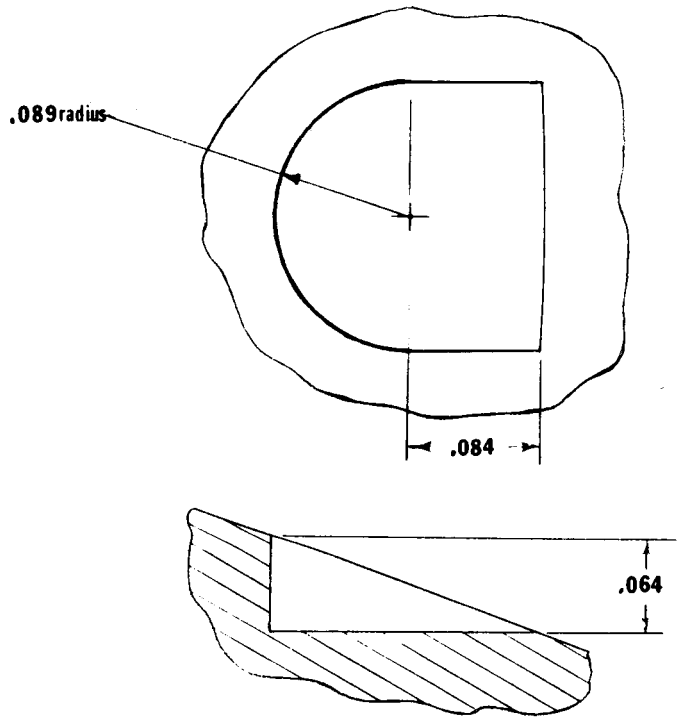

ATTACHMENT POINT A

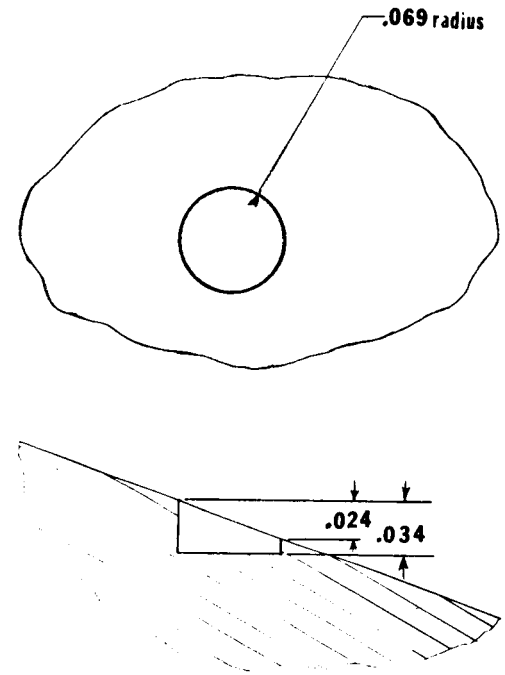

ATTACHMENT POINT B

Figure 2.- Details of aeroshell-bioshield attachment points. All dimensions are in centimeters.

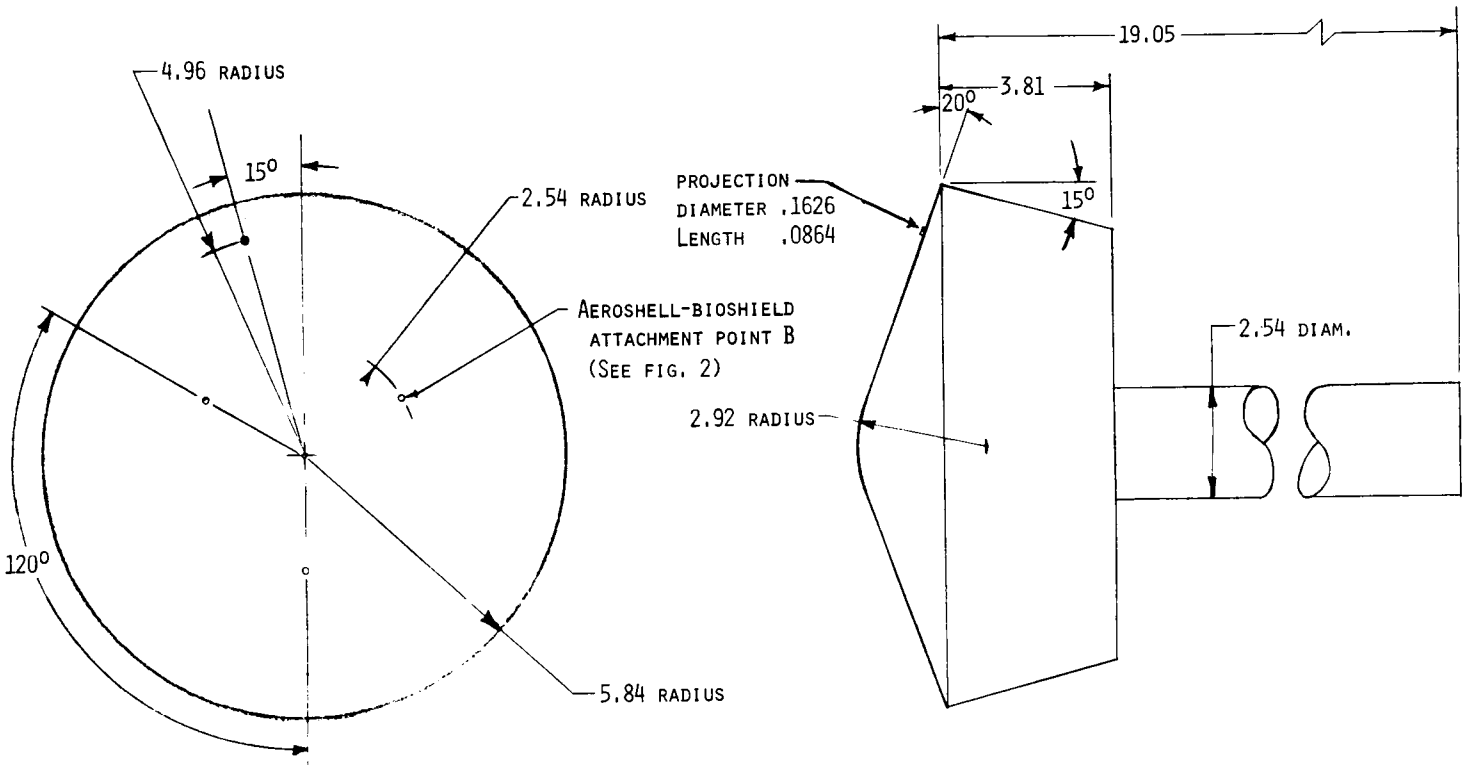

Figure 3.- Schematic of model 5 of Mars entry vehicle. All linear dimensions are in centimeters.

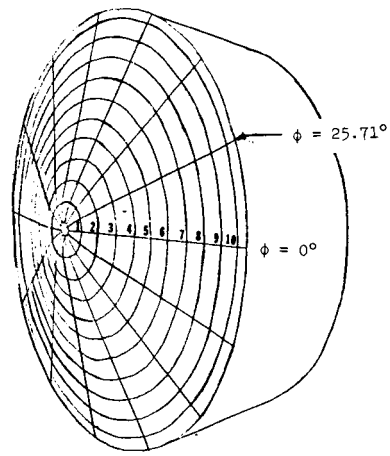

Grid model 1

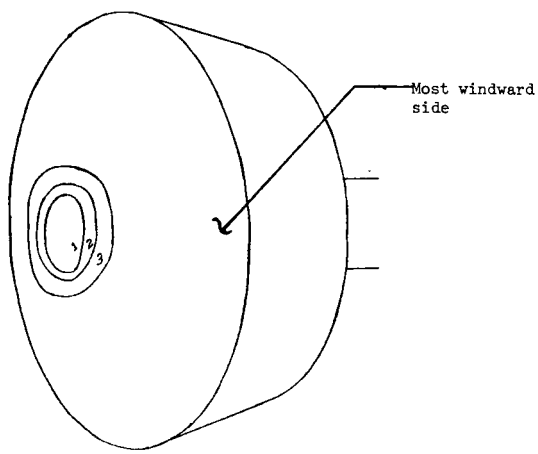

R/M= 4.00938E+00
HS= 2.23473E+02

CONTOUR	T, SEC	H/HS
1	4.60	8.83650E-01
2	7.70	7.02363E-01
3	9.60	6.37593E-01

MODEL 1

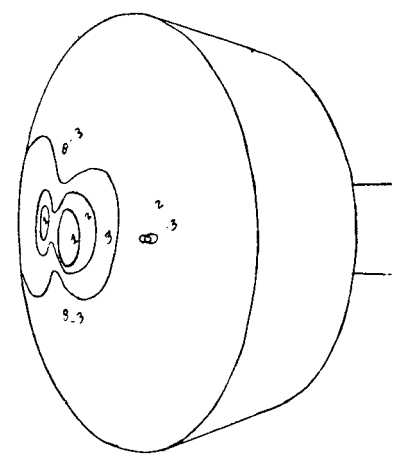

R/M= 1.61557E+07
HS= 4.92540E+02

CONTOUR	T, SEC	H/HS
1	3.40	9.51596E-01
2	4.90	7.98727E-01
3	6.70	6.68732E-01

MODEL 4

(a) Models 1 and 4.

Figure 4.- Heat-transfer data for four models of Mars entry vehicle at $\alpha = 3^{o}$. Top view.

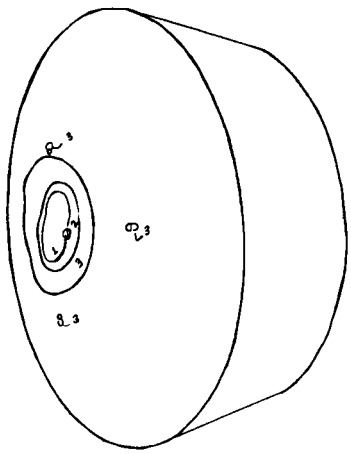

R/M= 4.09700E+06
HS= 2.23380E+02

CONTOUR	T,SEC	H/HS
1	4.10	9.02702E-01
2	5.60	7.75851E-01
3	8.60	6.33143E-01

MODEL 3

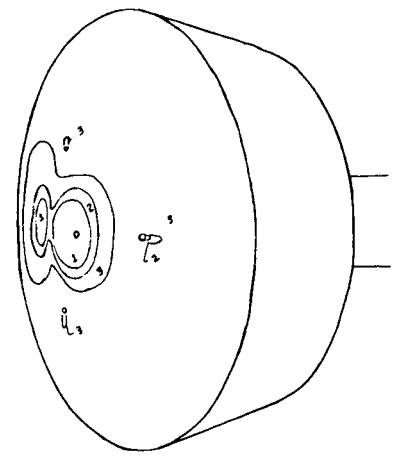

R/M= 1.60231E+07
HS= 4.90570E+02

CONTOUR	T,SEC	H/HS
1	4.00	8.92048E-01
2	5.10	7.96058E-01
3	8.20	6.35919E-01

MODEL 3

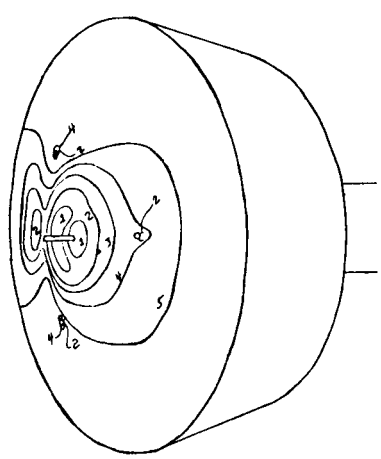

R/M= 1.62500E+07
HS= 4.92369E+02

CONTOUR	T,SEC	H/HS
1	2.20	1.22067E+00
2	3.80	9.28790E-01
3	5.30	8.00694E-01
4	6.60	7.21251E-01
5	8.80	6.37908E-01

MODEL 2

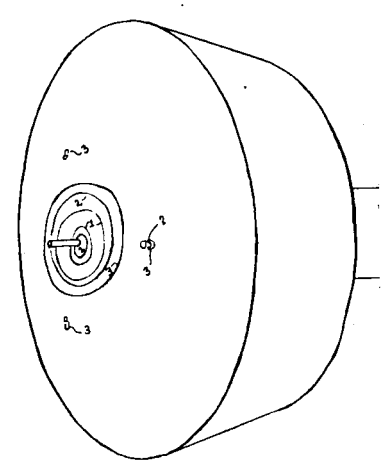

R/M= 3.96834E+06
HS= 2.23758E+02

CONTOUR	T,SEC	H/HS
1	3.10	1.01772E+00
2	5.10	7.93455E-01
3	7.10	6.85943E-01

MODEL 2

(b) Models 2 and 3.

Figure 4.- Continued.

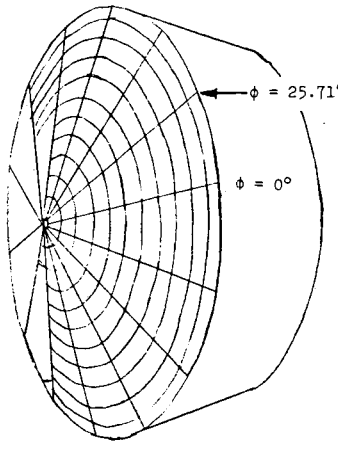

Grid model 1

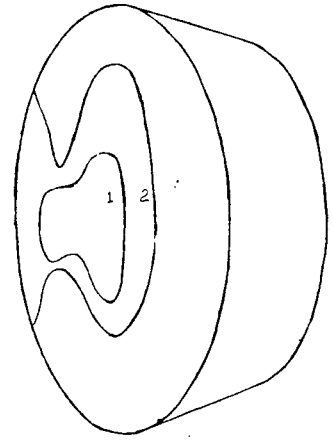

R/M= 1.72845E+07
HS= 4.95994E+02

CONTOUR	T,SEC	H/HS
1	7.10	7.54844E-01
2	11.70	5.99174E-01

MODEL 1

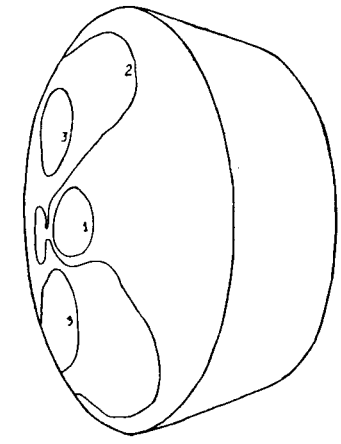

R/M= 3.73682E+06
HS= 2.24669E+02

CONTOUR	T,SEC	H/HS
1	4.90	7.78063E-01
2	7.00	6.55081E-01
3	10.50	5.42862E-01

MODEL 1

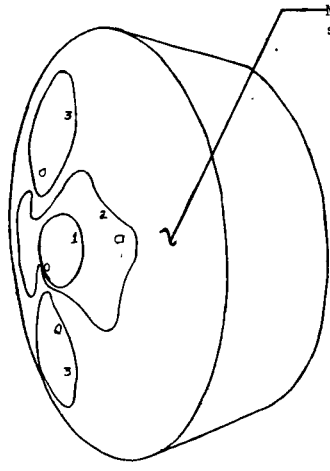

R/M= 3.82488E+06
HS= 2.21685E+02

CONTOUR	T,SEC	H/HS
1	4.20	8.39484E-01
2	7.00	6.53084E-01
3	9.30	5.76612E-01

MODEL 4

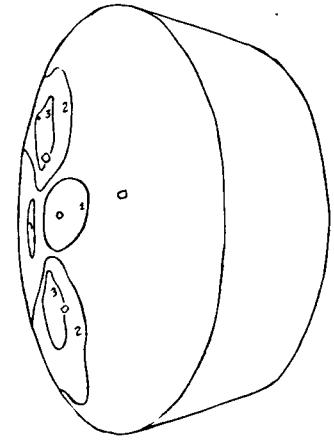

R/M= 3.58674E+06
HS= 2.22572E+02

CONTOUR	T,SEC	H/HS
1	4.30	7.55919E-01
2	5.80	6.54929E-01
3	9.50	5.13872E-01

MODEL 3

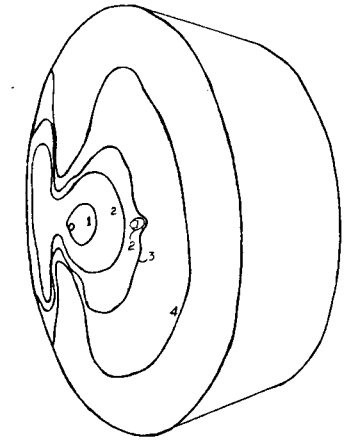

R/M= 1.67980E+07
HS= 4.89188E+02

CONTOUR	T,SEC	H/HS
1	5.70	8.04645E-01
2	9.60	6.18373E-01
3	10.80	5.89274E-01
4	14.60	5.06818E-01

MODEL 3

(c) Models 1, 3, and 4.

Figure 4.- Concluded.

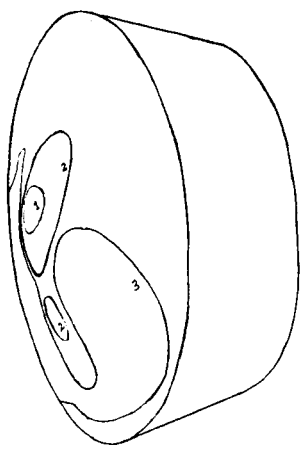

R/M= 3.73662E+06
HS= 2.24669E+02

CONTOUR	T,SEC	H/HS
1	5.80	7.14109E-01
2	7.20	6.48372E-01
3	8.60	5.88817E-01

MODEL 1

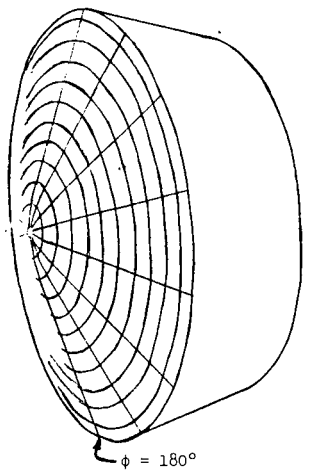

Grid model 1

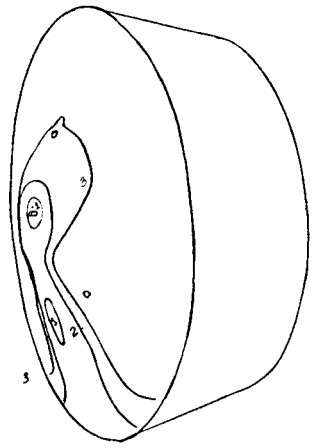

R/M= 3.82488E+06
HS= 2.21685E+02

CONTOUR	T,SEC	H/HS
1	3.80	8.79332E-01
2	6.20	6.97574E-01
3	7.80	6.24378E-01

MODEL 3

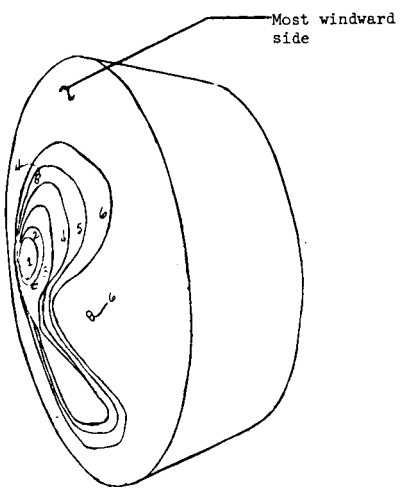

R/M= 3.58674E+06
HS= 2.22572E+02

CONTOUR	T,SEC	H/HS
1	4.30	7.54828E-01
2	5.40	6.73852E-01
3	6.30	6.33935E-01
4	6.70	6.14721E-01
5	7.70	5.73416E-01
6	8.70	5.39455E-01

MODEL 4

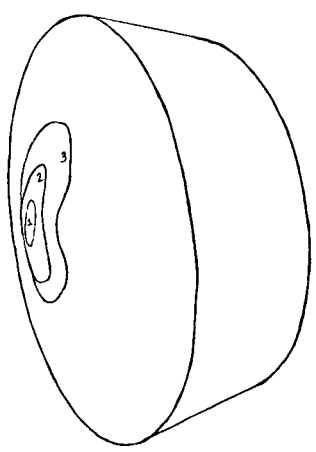

R/M= 1.72845E+07
HS= 4.95994E+02

CONTOUR	T,SEC	H/HS
1	5.80	8.33614E-01
2	8.00	7.24997E-01
3	10.40	6.35864E-01

MODEL 1

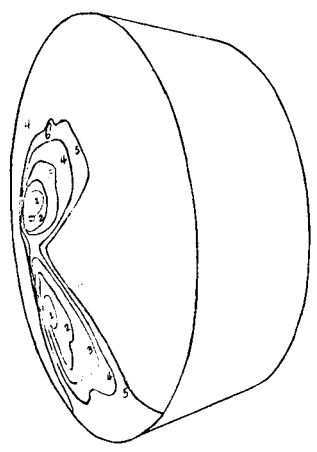

R/M= 1.67980E+07
HS= 4.89188E+02

CONTOUR	T,SEC	H/HS
1	6.70	7.38825E-01
2	8.10	6.72127E-01
3	9.30	6.27434E-01
4	10.40	6.05709E-01
5	11.20	5.83676E-01

MODEL 3

(a) Models 1, 2, and 3.

Figure 5.- Heat-transfer data for four models of Mars entry vehicle at $\alpha = 3^{o}$. Side view.

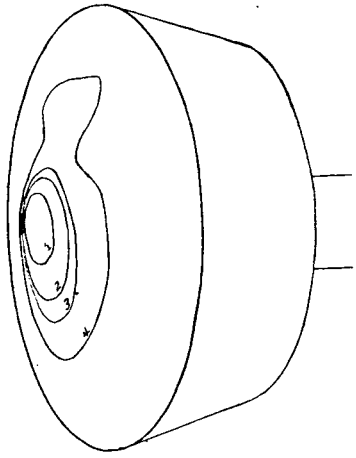

R/M= 4.06938E+06
HS= 2.23475E+02

CONTOUR	T,SEC	H/HS
1	5.90	7.95792E-01
2	8.80	6.57295E-01
3	9.50	6.36894E-01
4	11.20	5.86570E-01

MODEL 1

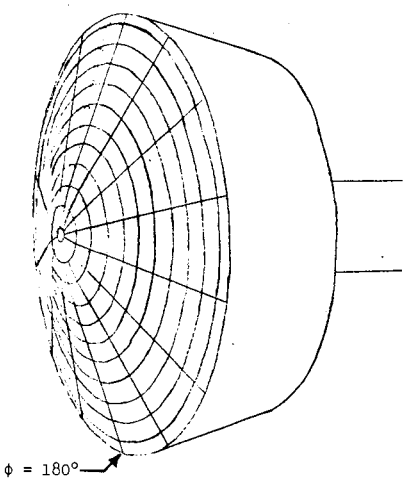

Grid model 1

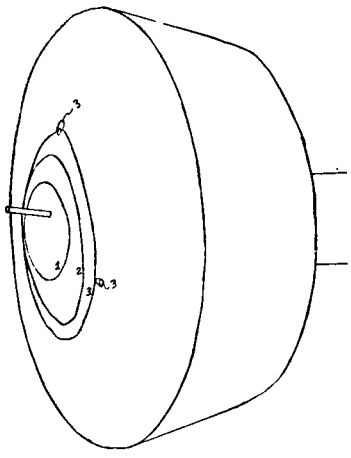

R/M= 3.98834E+06
HS= 2.23758E+02

CONTOUR	T,SEC	H/HS
1	6.40	7.17375E-01
2	8.50	6.25800E-01
3	9.50	5.91948E-01

MODEL 2

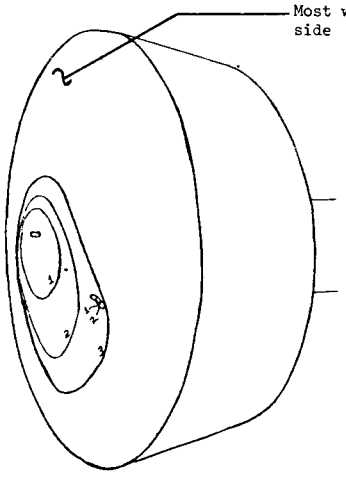

R/M= 4.09700E+06
HS= 2.23380E+02

CONTOUR	T,SEC	H/HS
1	6.50	7.21427E-01
2	8.80	6.27609E-01
3	10.30	5.80112E-01

MODEL 3

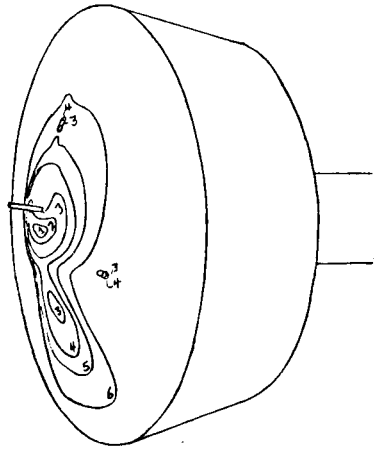

R/M= 1.62500E+07
HS= 4.92369E+02

CONTOUR	T,SEC	H/HS
1	2.70	1.10270E+00
2	3.20	1.01213E+00
3	4.20	8.84129E-01
4	5.20	8.10875E-01
5	6.30	7.36691E-01

MODEL 2

(b) Models 1, 2, and 3.

Figure 5.- Continued.

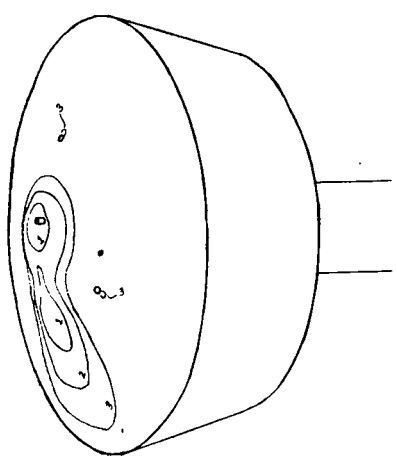

R/M= 1.60231E+07
HS= 4.90579E+02

CONTOUR	T,SEC	H/HS
1	4.90	8.06585E-01
2	7.00	6.80529E-01
3	9.10	6.02407E-01

MODEL 3

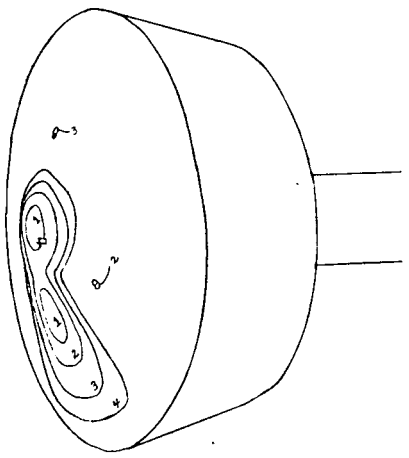

R/M= 1.61557E+07
HS= 4.92540E+02

CONTOUR	T,SEC	H/HS
1	4.40	8.40535E-01
2	5.70	7.40181E-01
3	7.60	6.45949E-01
4	8.90	6.00610E-01

MODEL 4

(c) Models 3 and 4.

Figure 5.- Concluded.

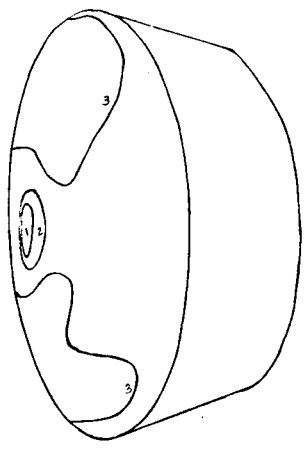

R/M= 3.77517E+06
HS= 2.21866E+02

CONTOUR	T,SEC	H/HS
1	3.50	9.17161E-01
2	5.40	7.38384E-01
3	9.90	5.51222E-01

MODEL 1

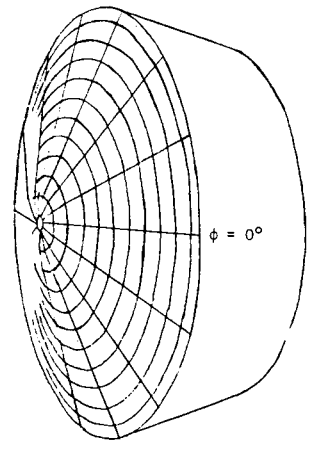

Grid model 1

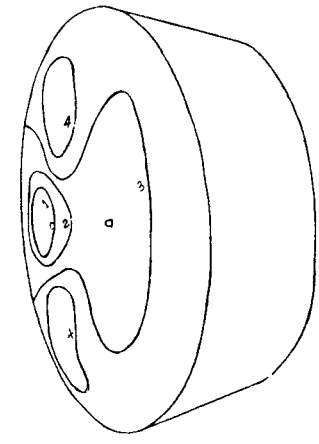

R/M= 4.04039E+06
HS= 2.25154E+02

CONTOUR	T,SEC	H/HS
1	4.40	8.24953E-01
2	6.50	6.80217E-01
3	8.80	5.89764E-01
4	11.20	5.27424E-01

MODEL 3

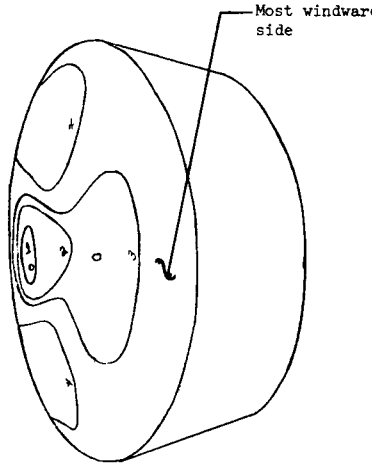

R/M= 3.71313E+06
HS= 2.24757E+02

CONTOUR	T,SEC	H/HS
1	3.60	8.35957E-01
2	6.20	6.39663E-01
3	7.60	5.80176E-01
4	10.10	5.09695E-01

MODEL 4

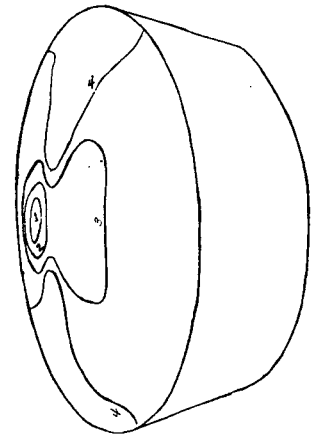

R/M= 1.67358E+07
HS= 4.91497E+02

CONTOUR	T,SEC	H/HS
1	3.00	1.14702E+00
2	5.70	8.29954E-01
3	7.40	7.30322E-01
4	10.50	6.19613E-01

MODEL 1

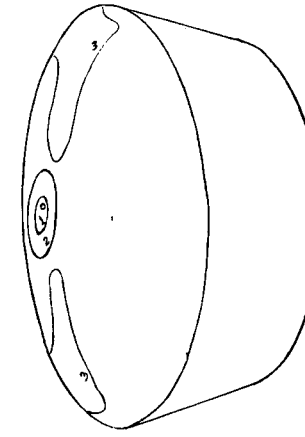

R/M= 1.63740E+07
HS= 4.91044E+02

CONTOUR	T,SEC	H/HS
1	3.00	1.04650E+00
2	5.80	7.50706E-01
3	9.60	5.94207E-01

MODEL 4

Figure 6.- Heat-transfer data for models 1, 3, and 4 of Mars entry vehicle at $\alpha = 6^{o}$. Top view.

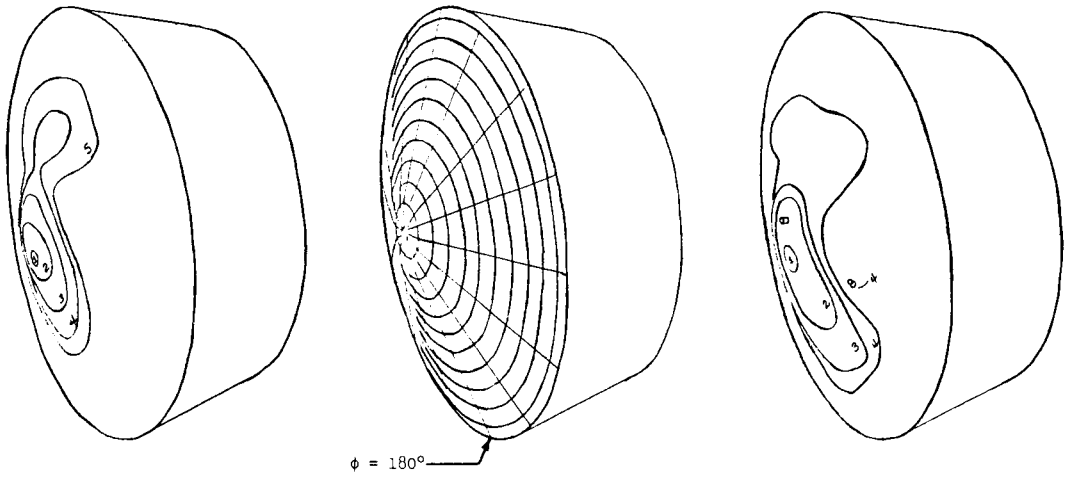

R/M= 3.77517E+06
HS= 2.21866E+02

CONTOUR	T,SEC	H/HS
1	4.00	9.09579E-01
2	5.50	7.69894E-01
3	7.50	6.60850E-01
4	9.00	6.11385E-01
5	10.00	5.80011E-01

MODEL 1

R/M= 4.04039E+06
HS= 2.25154E+02

CONTOUR	T,SEC	H/HS
1	3.70	9.02565E-01
2	6.80	6.65771E-01
3	7.90	6.26878E-01
4	9.00	5.87321E-01

MODEL 3

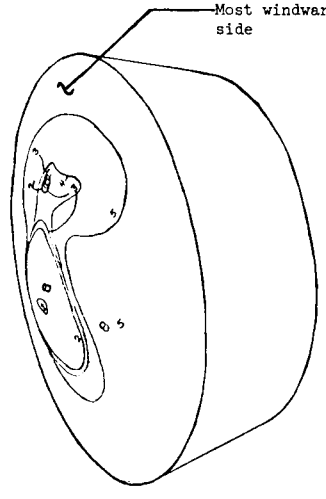

R/M= 3.71313E+06
HS= 2.24757E+02

CONTOUR	T,SEC	H/HS
1	3.30	8.79721E-01
2	6.50	6.26823E-01
3	6.80	6.16591E-01
4	7.00	6.08618E-01
5	10.00	5.09206E-01

MODEL 4

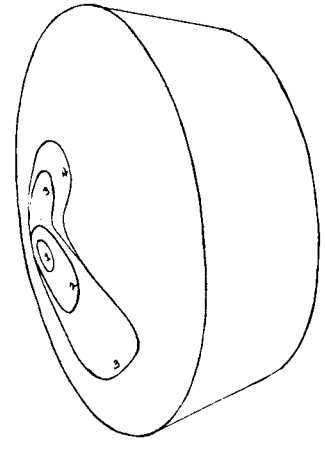

R/M= 1.67358E+07
HS= 4.91497E+02

CONTOUR	T,SEC	H/HS
1	4.30	9.54469E-01
2	5.90	8.12912E-01
3	8.20	7.02258E-01
4	9.90	6.40324E-01

MODEL 1

(a) Models 1, 3, and 4.

Figure 7.- Heat-transfer data for three models of Mars entry vehicle at $\alpha = 6^{\circ}$. Side view.

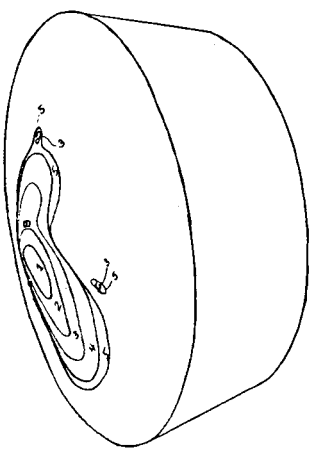

R/M= 1.70105E+07
HS= 4.95385E+02

CONTOUR	T,SEC	H/HS
1	4.40	8.79681E-01
2	5.60	7.78529E-01
3	7.70	6.71137E-01
4	9.00	6.27591E-01
5	9.70	6.04522E-01

MODEL 3

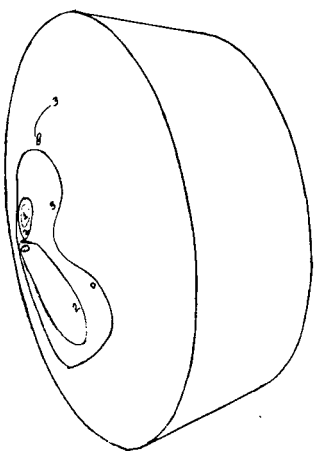

R/M= 1.63740E+07
HS= 4.91044E+02

CONTOUR	T,SEC	H/HS
1	3.00	1.04381E+00
2	4.90	8.18006E-01
3	8.60	6.29784E-01

MODEL 4

(b) Models 3 and 4.

Figure 7.- Concluded.

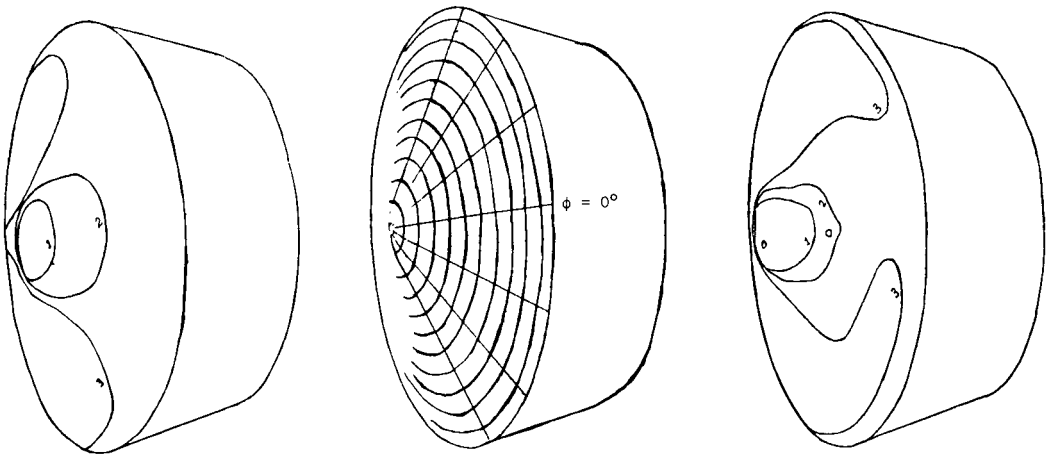

R/M= 3.90997E+06
HS= 2.24036E+02

CONTOUR	T,SEC	H/HS
1	3.20	9.79043E-01
2	4.70	8.11339E-01
3	6.30	7.00779E-01

MODEL 1

Grid model 1

R/M= 3.75072E+06
HS= 2.21956E+02

CONTOUR	T,SEC	H/HS
1	7.20	6.18250E-01
2	8.20	5.80559E-01
3	10.10	5.26469E-01

MODEL 4

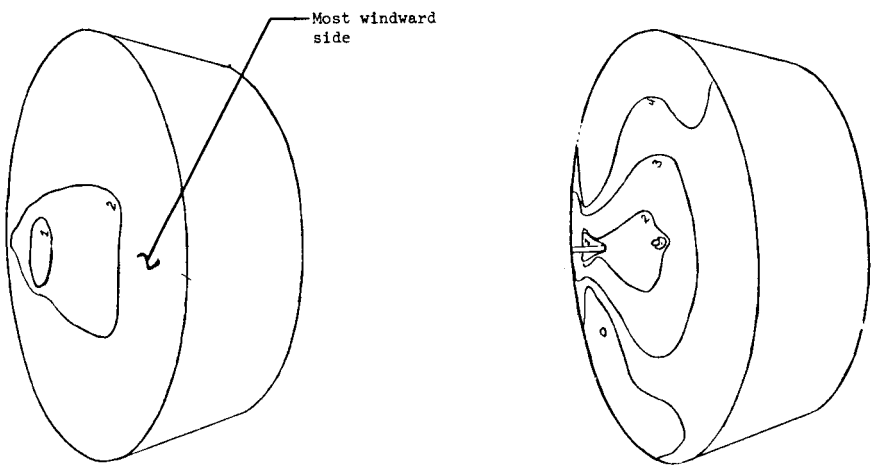

R/M= 1.63235E+07
HS= 4.85600E+02

CONTOUR	T,SEC	H/HS
1	5.10	8.85896E-01
2	7.00	7.56169E-01

MODEL 1

R/M= 1.69370E+07
HS= 4.91583E+02

CONTOUR	T,SEC	H/HS
1	3.40	8.32586E-01
2	3.80	7.85636E-01
3	5.30	6.66854E-01
4	6.80	5.91607E-01

MODEL 2

(a) Models 1, 2, and 4.

Figure 8.- Heat-transfer data for four models of Mars entry vehicle at $\alpha = 9^{o}$. Top view.

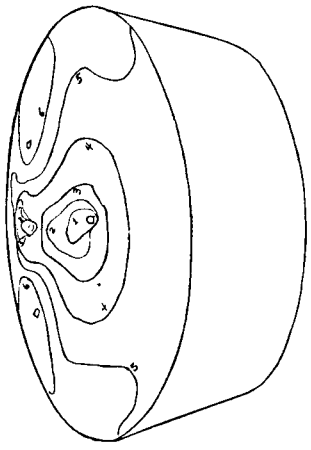

R/M= 1.72093E+07
HS= 4.68909E+02

CONTOUR	T, SEC	H/HS
1	3.70	8.15096E-01
2	4.20	7.65041E-01
3	4.90	7.08291E-01
4	6.20	6.28108E-01
5	7.80	5.62788E-01
6	10.80	4.81885E-01

MODEL 3

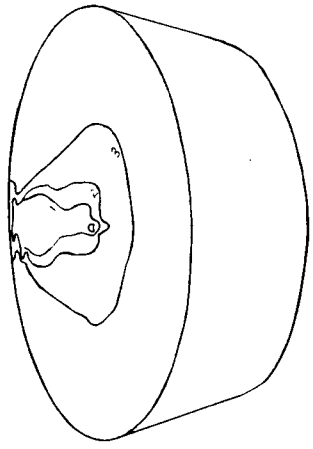

R/M= 1.63235E+07
HS= 4.85600E+02

CONTOUR	T, SEC	H/HS
1	7.30	6.99148E-01
2	8.20	6.59665E-01
3	10.40	5.87289E-01

MODEL 4

(b) Models 3 and 4.

Figure 8.- Continued.

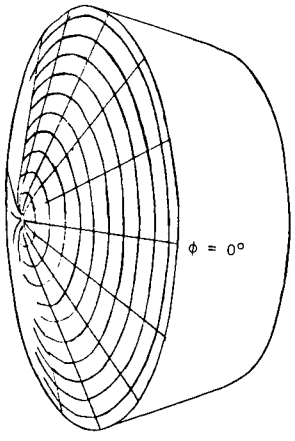

Grid model 1

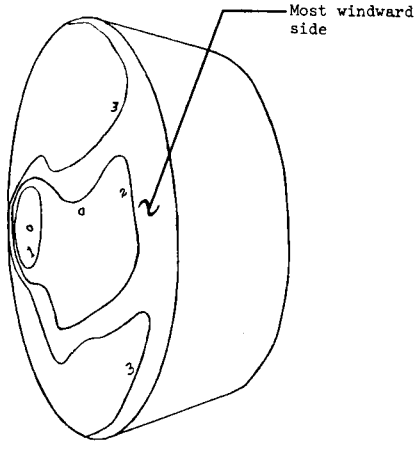

R/M= 4.26566E+06
HS= 2.24385E+02

CONTOUR	T,SEC	H/HS
1	5.60	7.76351E-01
2	10.40	5.72294E-01
3	12.20	5.33275E-01

MODEL 3

(c) Model 3.

Figure 8.- Concluded.

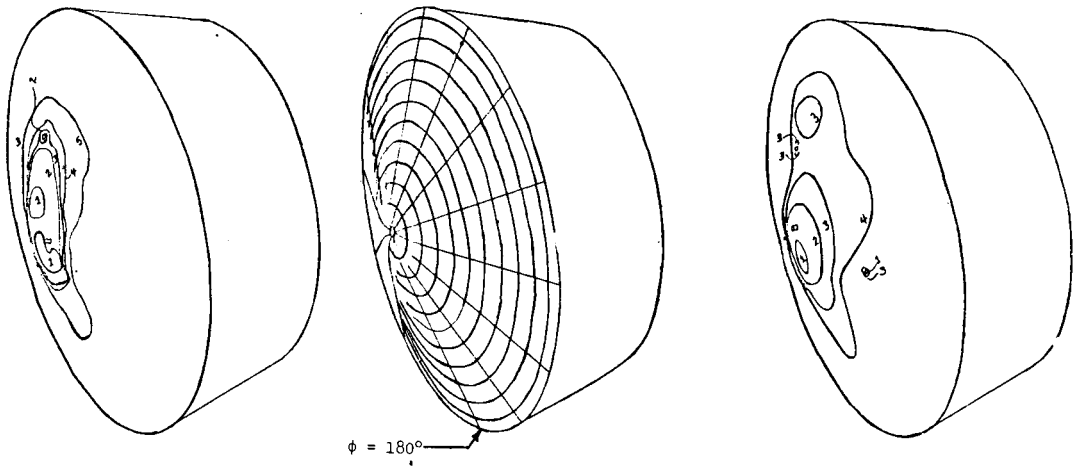

R/M= 3.75072E+06
HS= 2.24950E+02
CONTOUR T,SEC H/HS
1 6.70 6.40904E-01
2 8.00 5.96914E-01
3 8.20 5.89590E-01
4 8.80 5.75715E-01
5 9.80 5.44906E-01

MODEL 4

Grid model 1

R/M= 4.26566E+06
HS= 2.24385E+02
CONTOUR T,SEC H/HS
1 6.10 7.43175E-01
2 7.40 6.76595E-01
3 10.10 5.87728E-01
4 11.10 5.60629E-01

MODEL 3

Most windward side

R/M= 1.63235E+07
HS= 4.65600E+02
CONTOUR T,SEC H/HS
1 7.60 7.39695E-01
2 8.60 6.95361E-01
3 9.70 6.54747E-01
4 11.10 6.12065E-01

MODEL 1

R/M= 1.63235E+07
HS= 4.65600E+02
CONTOUR T,SEC H/HS
1 7.00 7.13973E-01
2 7.40 7.09646E-01
3 7.90 6.86821E-01
4 8.60 6.58276E-01
5 9.50 6.26319E-01

MODEL 4

(a) Models 1, 3, and 4.

Figure 9.- Heat-transfer data for three models of Mars entry vehicle at $\alpha = 9^{\circ}$. Side view.

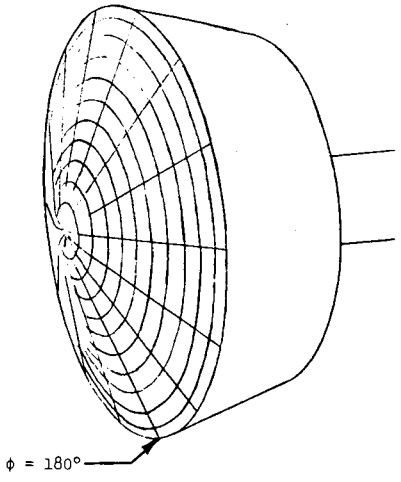

Grid model 1

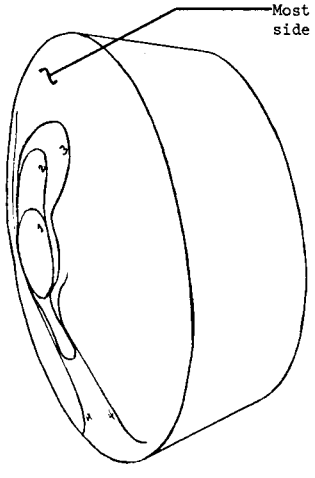

R/M= 3.90997E+06
HS= 2.24036E+02

CONTOUR	T,SEC	H/HS
1	3.70	9.18603E-01
2	5.30	7.74422E-01
3	6.10	7.21856E-01
4	7.20	6.64430E-01

MODEL 1

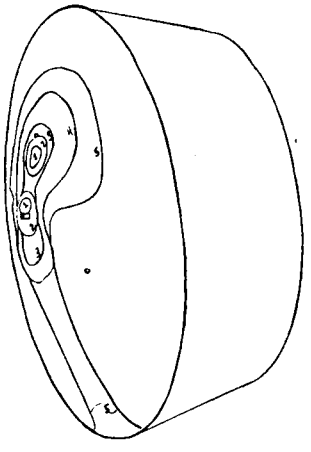

R/M= 1.72093E+07
HS= 4.88909E+02

CONTOUR	T,SEC	H/HS
1	4.00	7.81988E-01
2	4.20	7.64280E-01
3	4.50	7.52591E-01
4	6.00	6.51763E-01
5	7.00	6.03415E-01

MODEL 3

(b) Models 1 and 3.

Figure 9.- Concluded.

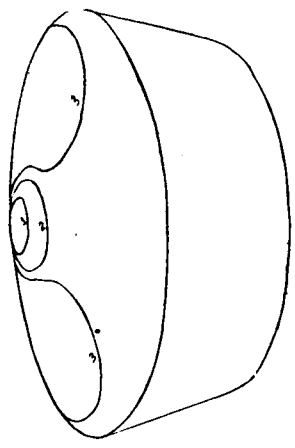

R/M= 3.85893E+06
HS= 2.22629E+02

CONTOUR	T,SEC	H/HS
1	3.10	1.01912E+00
2	4.30	8.67179E-01
3	5.70	7.58097E-01

MODEL 1

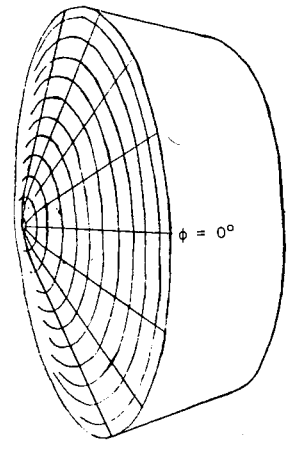

Grid model 1

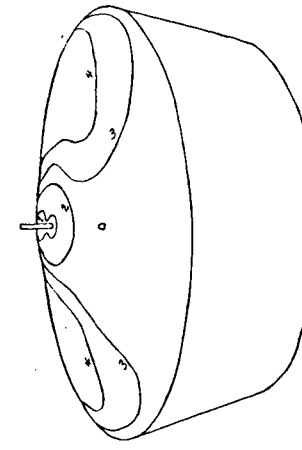

R/M= 4.08903E+06
HS= 2.22350E+02

CONTOUR	T,SEC	H/HS
1	2.90	1.09254E+00
2	4.60	8.65531E-01
3	6.50	7.29759E-01
4	8.60	6.41645E-01

MODEL 2

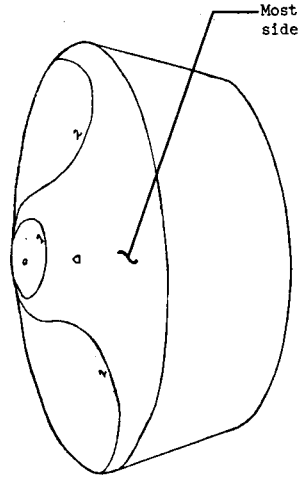

R/M= 3.90154E+06
HS= 2.21409E+02

CONTOUR	T,SEC	H/HS
1	3.50	9.37147E-01
2	5.30	7.68281E-01

MODEL 3

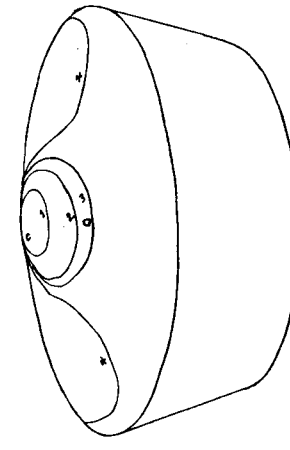

R/M= 3.84191E+06
HS= 2.22157E+02

CONTOUR	T,SEC	H/HS
1	2.80	1.01558E+00
2	4.60	7.55767E-01
3	5.30	7.44574E-01
4	6.10	6.95544E-01

MODEL 4

(a) Reynolds number per meter $\approx 3.7 \times 10^6$.

Figure 10.- Heat-transfer data for four models of Mars entry vehicle at $\alpha = 12^0$. Top view.

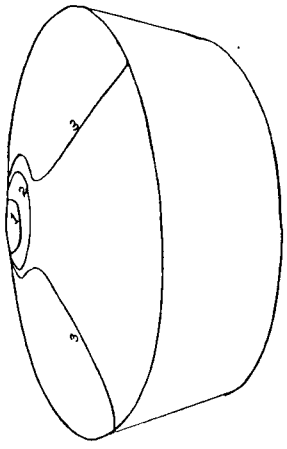

R/M= 1.67980E+07
HS= 4.89188E+02

CONTOUR	T,SEC	H/HS
1	3.50	1.08732E+00
2	5.80	8.42410E-01
3	8.10	7.18560E-01

MODEL 1

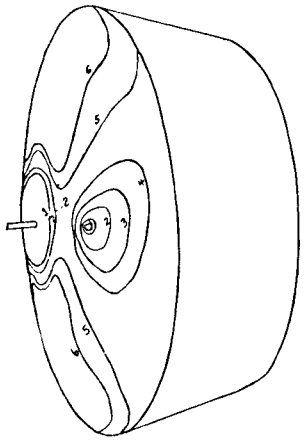

R/M= 1.64028E+07
HS= 4.90329E+02

CONTOUR	T,SEC	H/HS
1	3.70	7.73131E-01
2	4.00	7.45349E-01
3	4.40	7.28059E-01
4	4.80	6.91980E-01
5	5.80	6.21950E-01
6	7.10	5.64847E-01

MODEL 2

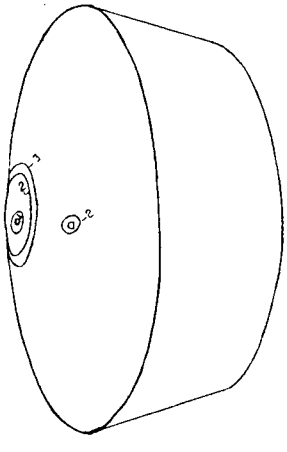

R/M= 1.64610E+07
HS= 4.87575E+02

CONTOUR	T,SEC	H/HS
1	2.30	1.23121E+00
2	4.30	8.98100E-01
3	6.60	7.26818E-01

MODEL 3

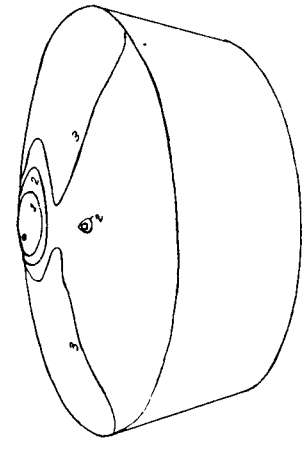

R/M= 1.64028E+07
HS= 4.89890E+02

CONTOUR	T,SEC	H/HS
1	3.40	9.89294E-01
2	5.30	7.94423E-01
3	8.10	6.44281E-01

MODEL 4

(b) Reynolds number per meter $\approx 17 \times 10^6$.

Figure 10.- Concluded.

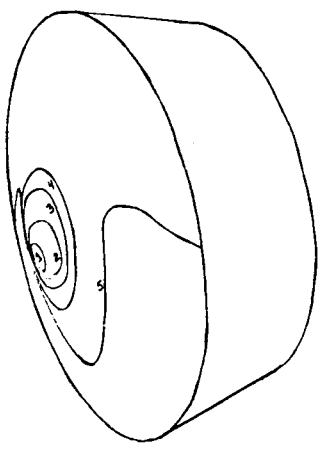

R/M= 3.85893E+06
HS= 2.22629E+02

CONTOUR	T,SEC	H/HS
1	3.40	9.76908E-01
2	4.10	8.86166E-01
3	5.20	7.89935E-01
4	6.20	7.33576E-01
5	7.60	6.62574E-01

MODEL 1

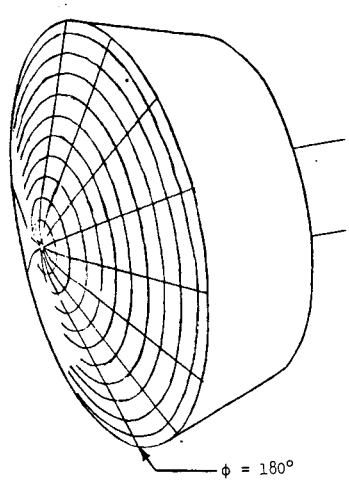

Grid model 1

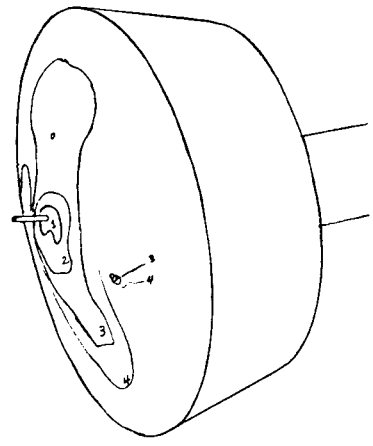

R/M= 4.08903E+06
HS= 2.22350E+02

CONTOUR	T,SEC	H/HS
1	3.60	9.76198E-01
2	4.70	8.57812E-01
3	7.30	6.98343E-01
4	9.50	6.12165E-01

MODEL 2

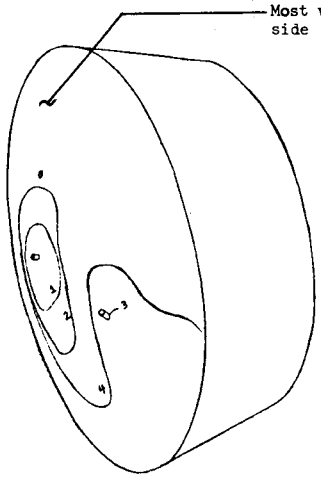

R/M= 3.90154E+06
HS= 2.21409E+02

CONTOUR	T,SEC	H/HS
1	3.80	9.00971E-01
2	6.10	7.21225E-01
3	7.00	6.73266E-01
4	7.80	6.37806E-01

MODEL 3

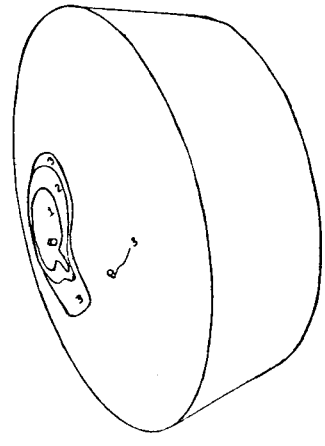

R/M= 3.84191E+06
HS= 2.22157E+02

CONTOUR	T,SEC	H/HS
1	3.20	9.53678E-01
2	4.60	8.06575E-01
3	5.50	7.376,36E-01

MODEL 4

(a) Reynolds number per meter $\approx 3.7 \times 10^6$.

Figure 11.- Heat-transfer data for four models of Mars entry vehicle at $\alpha = 12^{\circ}$. Side view.

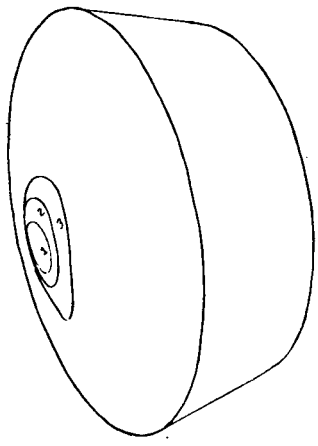

R/M= 1.67980E+07
HS= 4.89188E+02

CONTOUR	T,SEC	H/HS
1	4.40	9.68730E-01
2	6.60	7.90964E-01
3	8.10	7.20679E-01

MODEL 1

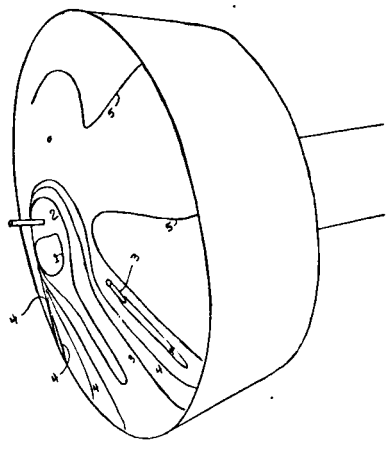

R/M= 1.64028E+07
HS= 4.90329E+02

CONTOUR	T,SEC	H/HS
1	2.30	5.62468E-01
2	4.00	7.44993E-01
3	6.20	5.98393E-01
4	8.00	5.34966E-01
5	10.30	4.71468E-01

MODEL 2

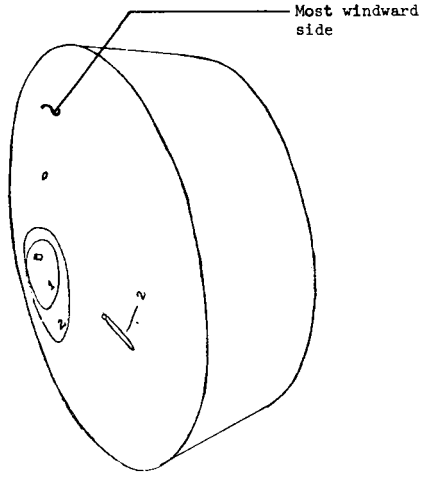

R/M= 1.64610E+07
HS= 4.87575E+02

CONTOUR	T,SEC	H/HS
1	3.60	9.81539E-01
2	7.30	6.92547E-01

MODEL 3

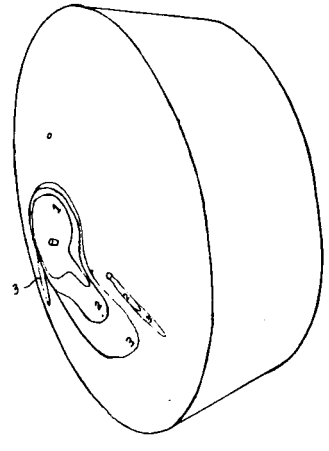

R/M= 1.64328E+07
HS= 4.89890E+02

CONTOUR	T,SEC	H/HS
1	5.10	8.09011E-01
2	6.90	6.96431E-01
3	8.20	6.41007E-01

MODEL 4

(b) Reynolds number per meter $\approx 17 \times 10^6$.

Figure 11.- Concluded.

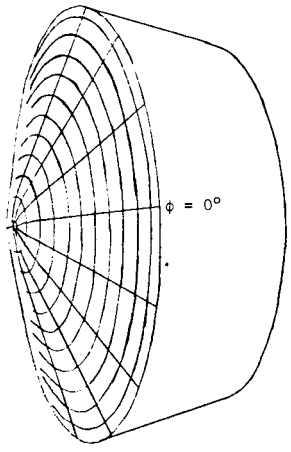

Grid model 1

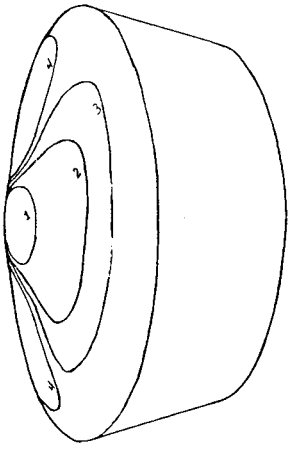

R/M= 4.07508E+06
HS= 2.26079E+02

CONTOUR	T,SEC	H/HS
1	3.00	1.06523E+00
2	3.60	9.72420E-01
3	5.70	7.74491E-01
4	7.00	6.98883E-01

MODEL 1

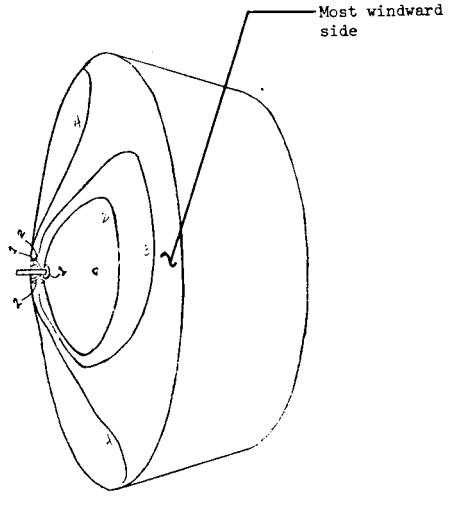

R/M= 4.03395E+06
HS= 2.22541E+02

CONTOUR	T,SEC	H/HS
1	2.20	1.24817E+00
2	3.20	1.03034E+00
3	4.20	8.99353E-01
4	5.40	7.91399E-01

MODEL 2

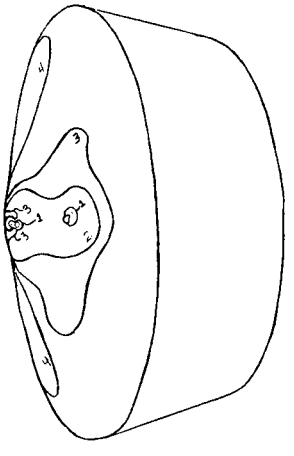

R/M= 4.03395E+06
HS= 2.22541E+02

CONTOUR	T,SEC	H/HS
1	3.00	1.05079E+00
2	3.60	9.57104E-01
3	4.60	8.46704E-01
4	7.10	6.80012E-01

MODEL 3

(a) Reynolds number per meter $\approx 3.7 \times 10^6$.

Figure 12.- Heat-transfer data for four models of Mars entry vehicle at $\alpha = 15^\circ$. Top view.

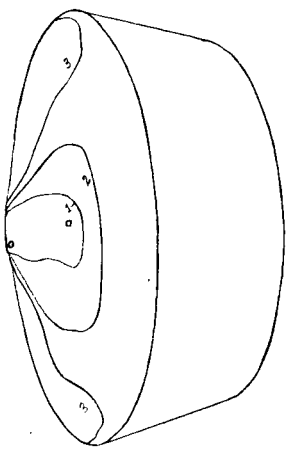

R/M= 3.97213E+06
HS= 2.20090E+02

CONTOUR	T,SEC	H/HS
1	3.40	1.01415E+00
2	4.40	8.89507E-01
3	5.90	7.68157E-01

MODEL 4

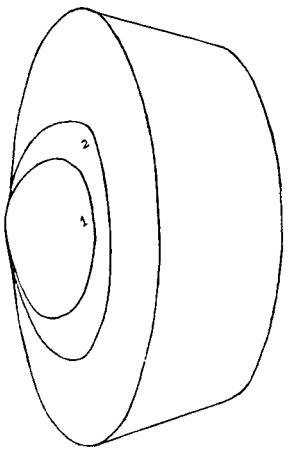

R/M= 1.65297E+07
HS= 4.88559E+02

CONTOUR	T,SEC	H/HS
1	5.60	8.46630E-01
2	7.10	7.53870E-01

MODEL 1

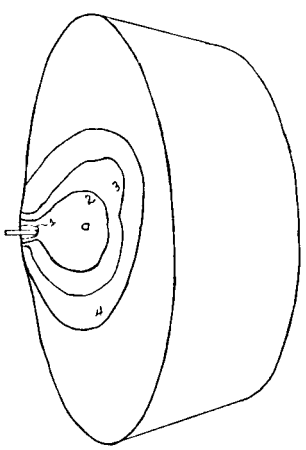

R/M= 1.65964E+07
HS= 4.89541E+02

CONTOUR	T,SEC	H/HS
1	1.60	1.51860E+00
2	3.70	9.96004E-01
3	5.00	8.56795E-01
4	7.00	7.22229E-01

MODEL 2

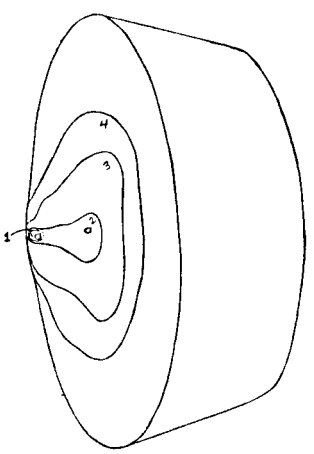

R/M= 1.65001E+07
HS= 4.89716E+02

CONTOUR	T,SEC	H/HS
1	2.30	1.23329E+00
2	3.60	9.83196E-01
3	5.30	8.08200E-01
4	8.50	6.36526E-01

MODEL 3

(b) Reynolds number per meter $\approx 17 \times 10^6$.

Figure 12.- Concluded.

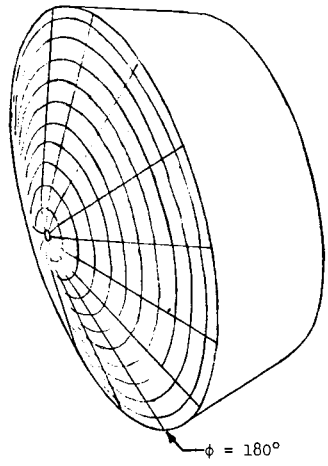

Grid model 1

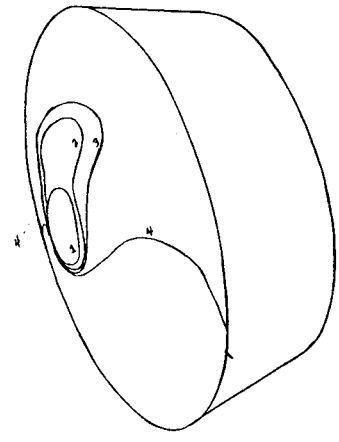

R/M= 4.07508E+06
HS= 2.26079E+02

CONTOUR	T,SEC	H/HS
1	4.30	8.92287E-01
2	5.20	8.23840E-01
3	5.90	7.73425E-01
4	8.60	6.40612E-01

MODEL 1

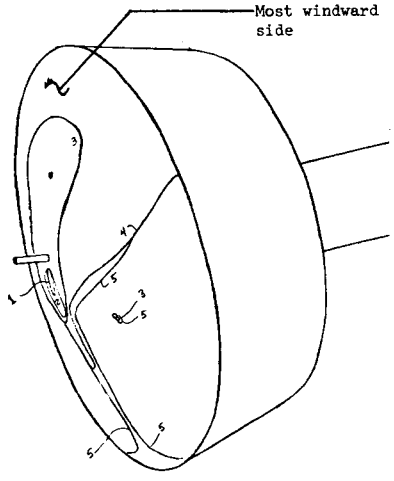

R/M= 4.03395E+06
HS= 2.22541E+02

CONTOUR	T,SEC	H/HS
1	1.60	1.46296E+00
2	3.70	9.62036E-01
3	4.20	9.13952E-01
4	5.70	7.84532E-01

MODEL 2

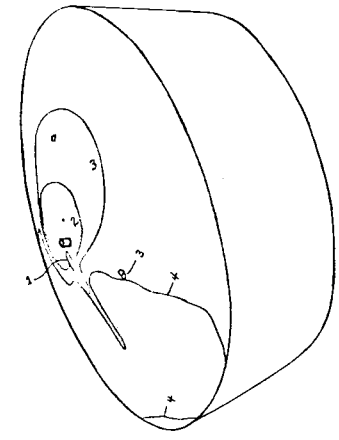

R/M= 3.97213E+06
HS= 2.20090E+02

CONTOUR	T,SEC	H/HS
1	2.80	1.11729E+00
2	4.70	8.62376E-01
3	6.00	7.75877E-01

MODEL 4

Figure 13.- Heat-transfer data for three models of Mars entry vehicle at a Reynolds number per meter of 3.7×10^6 at $\alpha = 15^\circ$. Side view.

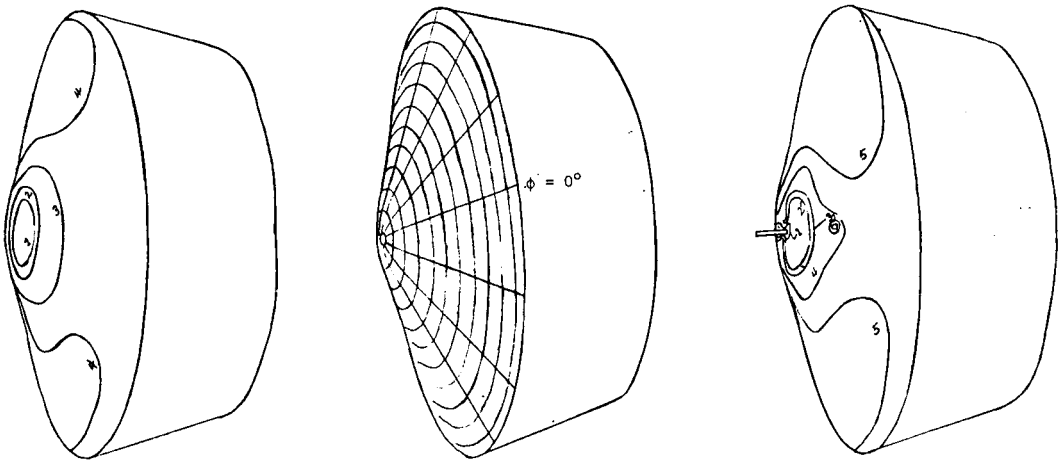

R/M= 4.00782E+06
HS= 2.21035E+02

CONTOUR	T,SEC	H/HS
1	3.00	1.13876E+00
2	4.20	9.62425E-01
3	6.10	7.91489E-01
4	7.90	6.57049E-01

MODEL 1

Grid model 1

R/M= 3.92766E+06
HS= 2.21317E+02

CONTOUR	T,SEC	H/HS
1	2.50	1.16601E+00
2	3.50	9.83281E-01
3	4.10	9.06490E-01
4	5.10	8.10989E-01
5	6.70	7.06008E-01

MODEL 2

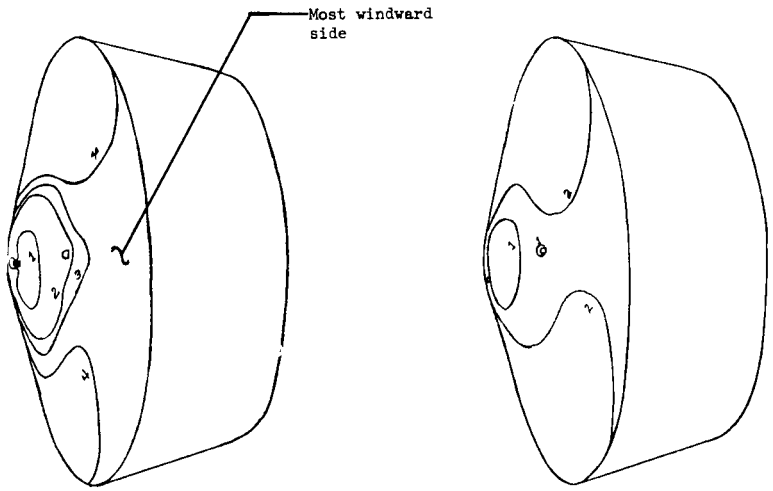

R/M= 3.92766E+06
HS= 2.21317E+02

CONTOUR	T,SEC	H/HS
1	3.00	1.04641E+00
2	4.30	8.68274E-01
3	4.50	8.48760E-01
4	5.10	8.04338E-01

MODEL 3

R/M= 3.90154E+06
HS= 2.21409E+02

CONTOUR	T,SEC	H/HS
1	3.00	1.03089E+00
2	4.20	8.63661E-01

MODEL 4

(a) Reynolds number per meter $\approx 3.7 \times 10^6$.

Figure 14.- Heat-transfer data for four models at Mars entry vehicle at $\alpha = 18^{\circ}$. Top view.

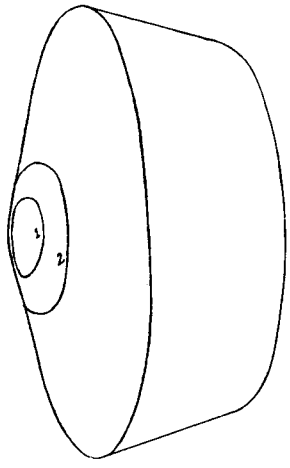

R/M= 1.60499E+07
HS= 4.89425E+02

CONTOUR	T,SEC	H/HS
1	3.10	1.09632E+00
2	4.70	8.85833E-01

MODEL 1

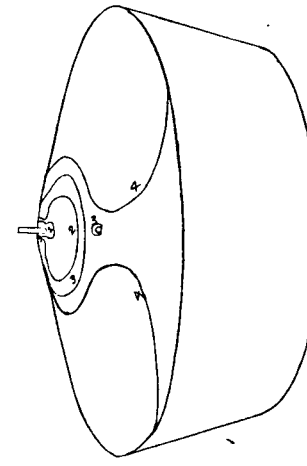

R/M= 1.62111E+07
HS= 4.90236E+02

CONTOUR	T,SEC	H/HS
1	2.00	1.30416E+00
2	3.00	1.06484E+00
3	4.20	8.90751E-01
4	6.20	7.36904E-01

MODEL 2

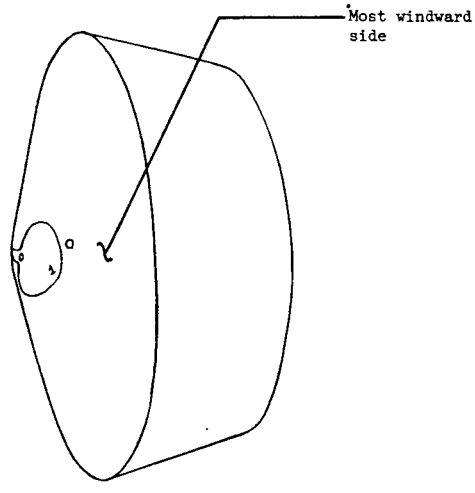

R/M= 1.60231E+07
HS= 4.90579E+02

CONTOUR	T,SEC	H/HS
1	3.20	9.99918E-01

MODEL 3

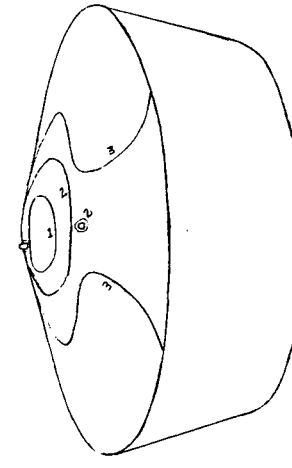

R/M= 1.62111E+07
HS= 4.90236E+02

CONTOUR	T,SEC	H/HS
1	3.00	1.05215E+00
2	4.30	8.69842E-01
3	6.10	7.35956E-01

MODEL 4

(b) Reynolds number per meter $\approx 17 \times 10^6$.

Figure 14.- Concluded.

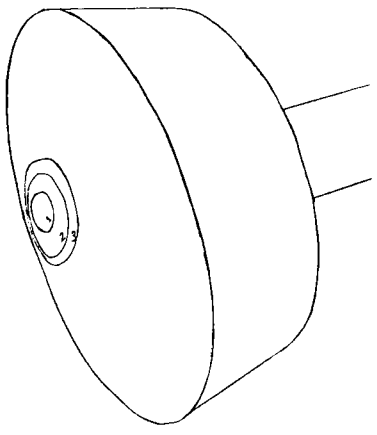

R/M= 4.00782E+06
HS= 2.21035E+02

CONTOUR	T,SEC	H/HS
1	4.70	9.01697E-01
2	6.10	8.06197E-01
3	7.30	7.36961E-01

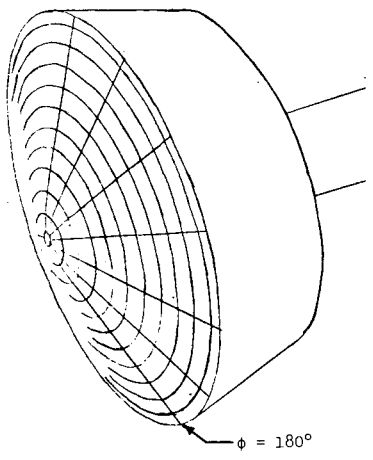

Grid model 1

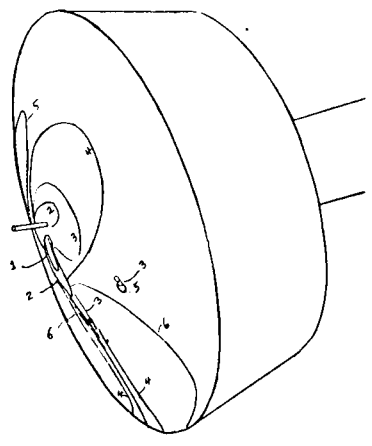

R/M= 3.92766E+06
HS= 2.21317E+02

CONTOUR	T,SEC	H/HS
1	2.50	1.16292E+00
2	4.40	8.71779E-01
3	5.20	8.09554E-01
4	7.50	6.79504E-01
5	8.60	6.34561E-01
6	11.40	5.51151E-01

MODEL 1

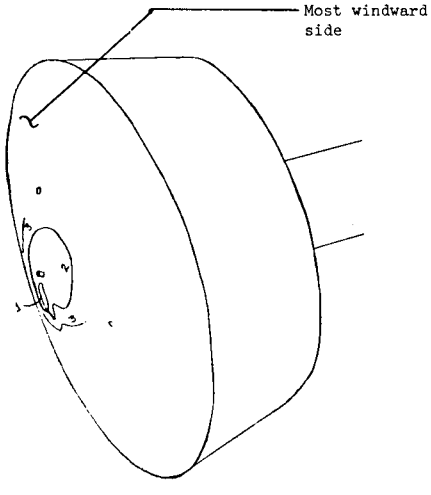

R/M= 3.92766E+06
HS= 2.21317E+02

CONTOUR	T,SEC	H/HS
1	3.40	9.74314E-01
2	4.60	8.40961E-01
3	6.50	7.17559E-01

MODEL 3

MODEL 2

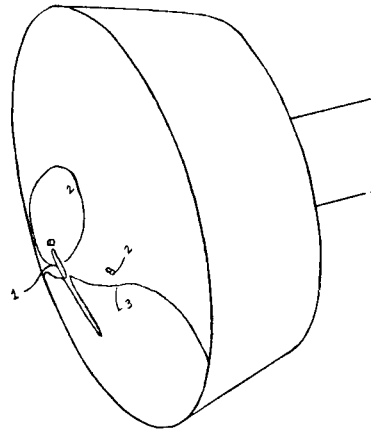

R/M= 3.90154E+06
HS= 2.21409E+02

CONTOUR	T,SEC	H/HS
1	3.00	1.02818E+00
2	4.80	8.22596E-01
3	7.20	6.71647E-01

MODEL 4

(a) Reynolds number per meter $\approx 3.7 \times 10^6$.

Figure 15.- Heat-transfer data for four models of Mars entry vehicle at $\alpha = 18^{\circ}$. Side view.

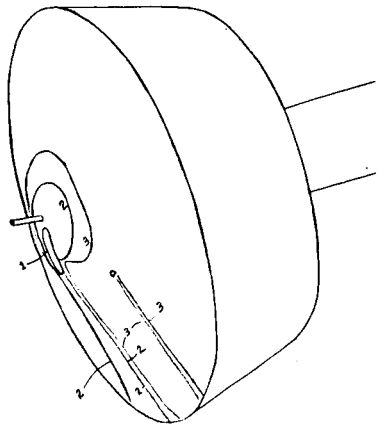

R/M= 1.62111E+07
HS= 4.90236E+02

CONTOUR	T,SEC	H/HS
1	2.20	1.23962E+00
2	4.90	8.25942E-01
3	6.80	7.15037E-01

MODEL 2

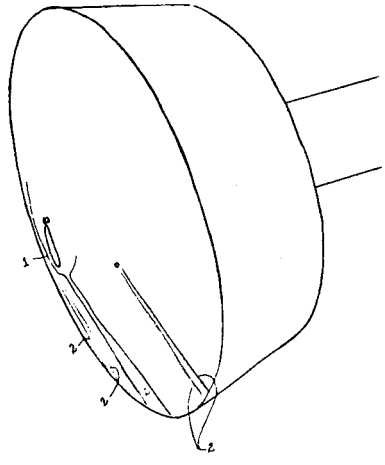

R/M= 1.60231E+07
HS= 4.90579E+02

CONTOUR	T,SEC	H/HS
1	2.20	1.19557E+00
2	7.90	6.43292E-01

MODEL 3

(b) Reynolds number per meter $\approx 17 \times 10^6$.

Figure 15.- Concluded.

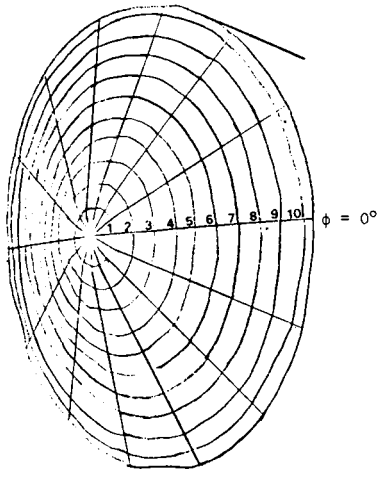

Grid model 1

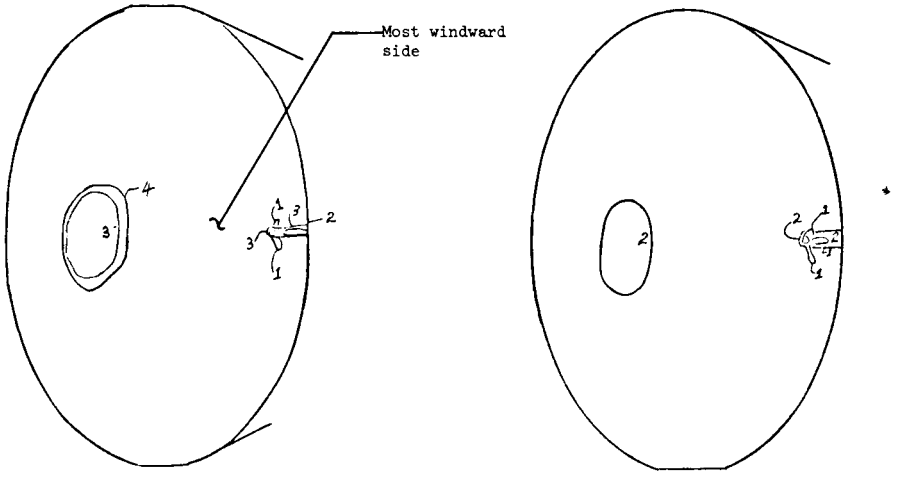

R/M= 3.92766E+06
HS= 2.21317E+02

CONTOUR	T,SEC	H/HS
1	.80	2.15104E+00
2	2.00	1.36082E+00
3	5.20	8.43743E-01
4	7.50	7.02723E-01

R/M= 1.68359E+07
HS= 4.91321E+02

CONTOUR	T,SEC	H/HS
1	.60	2.54952E+00
2	4.40	9.41474E-01

(a) $\alpha = 0^{o}$.

Figure 16.- Heat-transfer data for model 5 of Mars entry vehicle at various angles of attack and two Reynolds numbers.

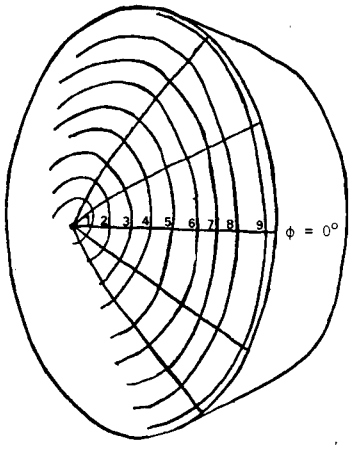

Grid model 2

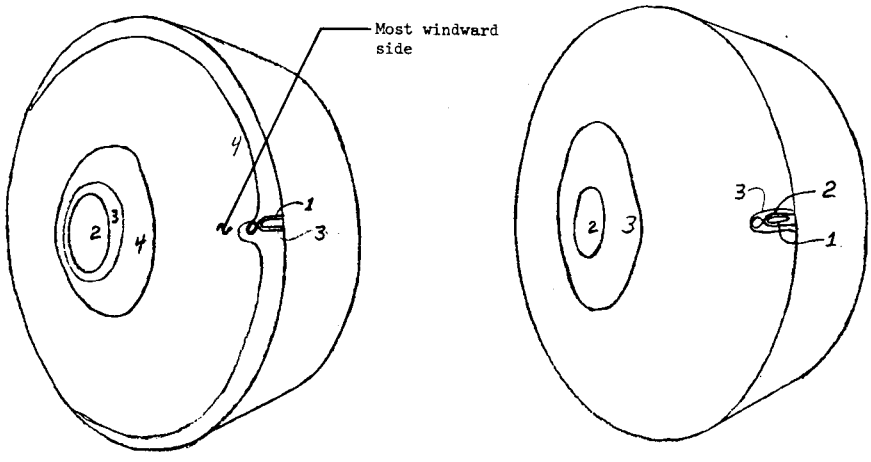

R/M= 3.90154E+06
HS= 2.21409E+02

CONTOUR	T,SEC	H/HS
1	4.50	9.18847E-01
2	6.10	7.89195E-01
3	7.90	6.93483E-01
4	10.60	5.98682E-01

R/M= 1.64414E+07
HS= 4.92023E+02

CONTOUR	T,SEC	H/HS
1	2.20	1.29393E+00
2	3.40	1.04064E+00
3	9.10	6.36214E-01

(b) $\alpha = 3^{o}$.

Figure 16.- Continued.

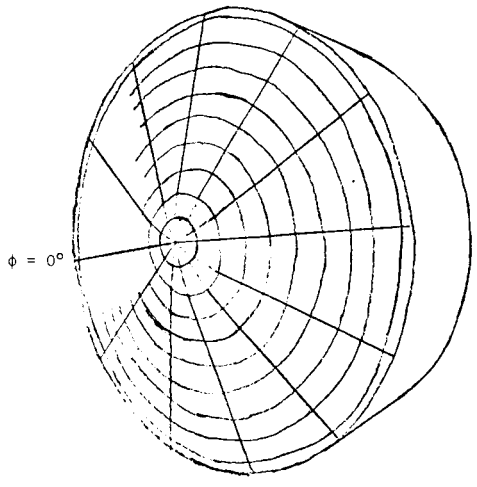

Grid model 2

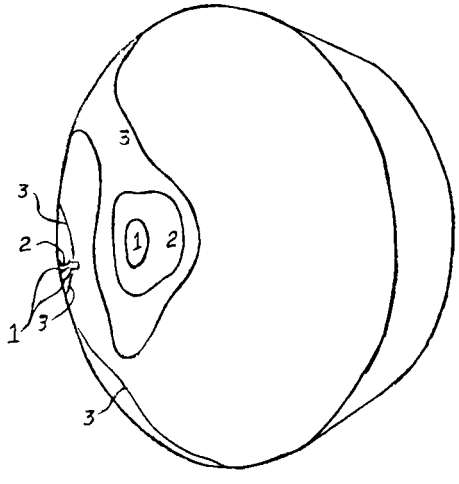

R/M= 3.82468E+06
HS= 2.21685E+02

CONTOUR	T,SEC	H/HS
1	5.10	8.13005E-01
2	6.50	7.20148E-01
3	8.60	6.26079E-01

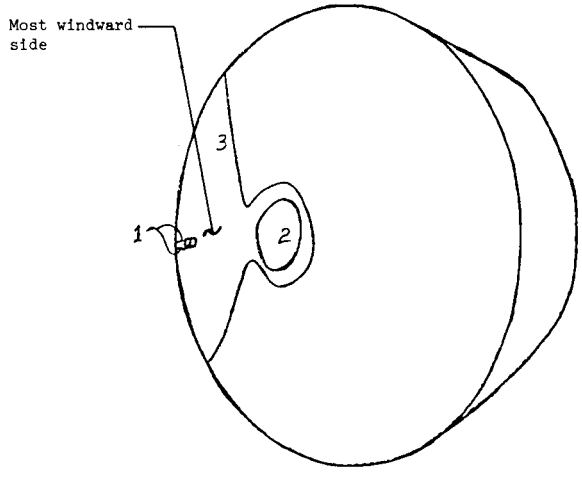

R/M= 1.66977E+07
HS= 4.89365E+02

CONTOUR	T,SEC	H/HS
1	2.00	1.41933E+00
2	4.70	9.25870E-01
3	6.40	7.93431E-01

(c) $\alpha = 6^{o}$.

Figure 16.- Continued.

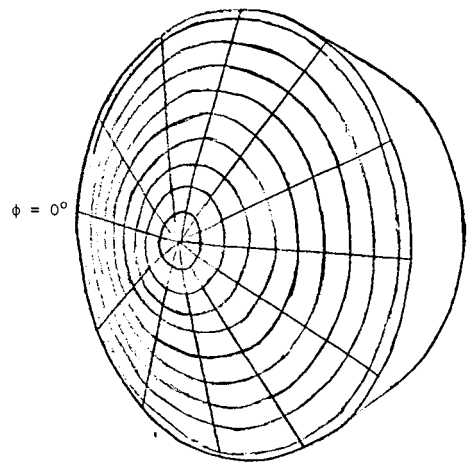

Grid model 2

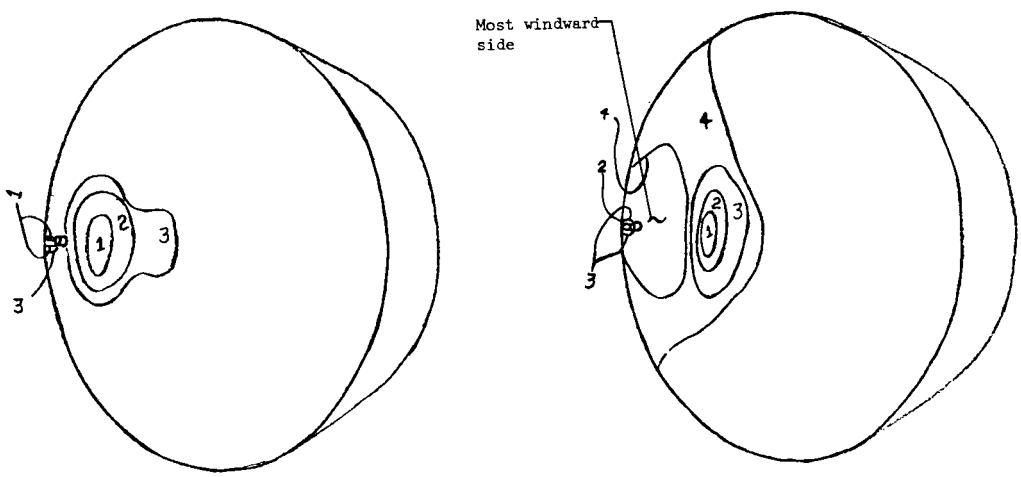

R/M= 3.90154E+06
HS= 2.21409E+02

CONTOUR	T,SEC	H/HS
1	4.20	9.35690E-01
2	6.10	7.76411E-01
3	7.30	7.09733E-01

R/M= 1.66977E+07
HS= 4.89365E+02

CONTOUR	T,SEC	H/HS
1	2.60	1.23573E+00
2	3.30	1.09686E+00
3	4.90	9.00142E-01
4	6.10	8.06759E-01

(d) $\alpha = 9^{o}$.

Figure 16.- Continued.

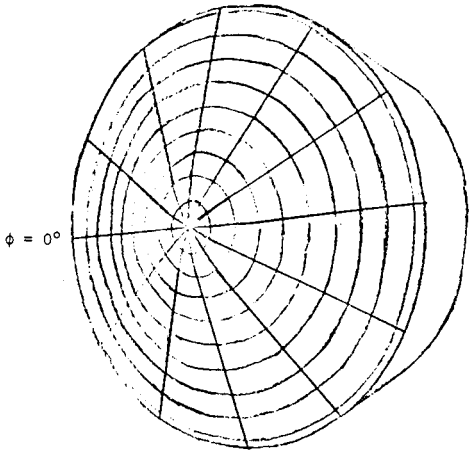

Grid model 2

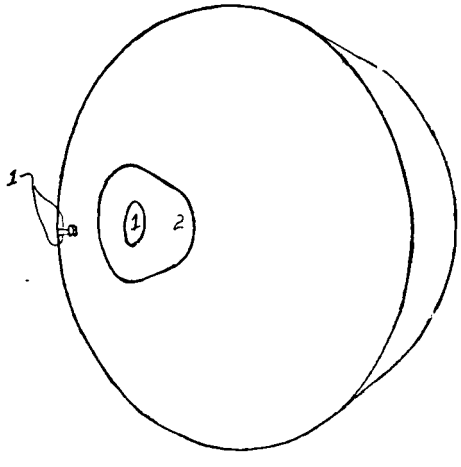

R/M= 3.65315E+06
HS= 2.21593E+02

CONTOUR	T, SEC	H/HS
1	4.40	9.32394E-01
2	7.80	7.00291E-01

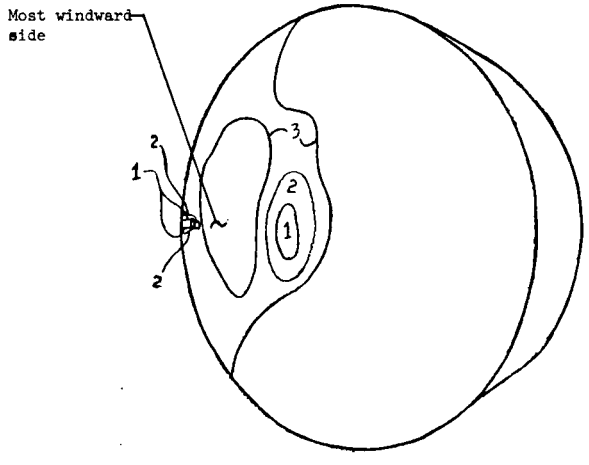

R/M= 1.66977E+07
HS= 4.89365E+02

CONTOUR	T, SEC	H/HS
1	3.00	1.16453E+00
2	4.10	9.96137E-01
3	5.90	8.30396E-01

(e) $\alpha = 12^{o}$.

Figure 16.- Continued.

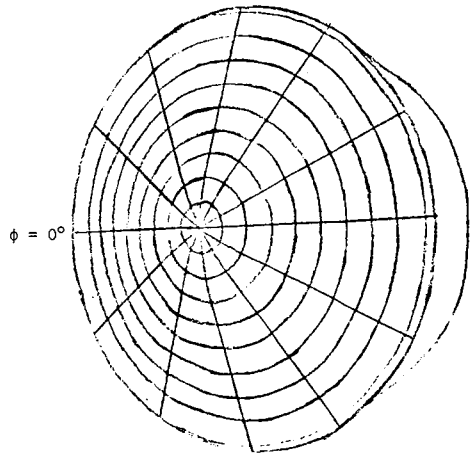

Grid model 2

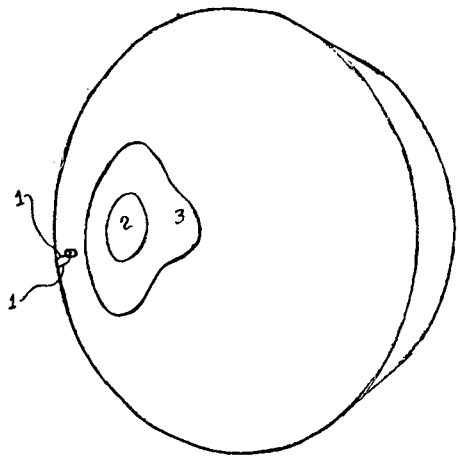

R/M= 4.00570E+06
HS= 2.23616E+02

CONTOUR	T,SEC	H/HS
1	.90	1.02480E+00
2	1.20	8.87501E-01
3	1.90	7.05314E-01

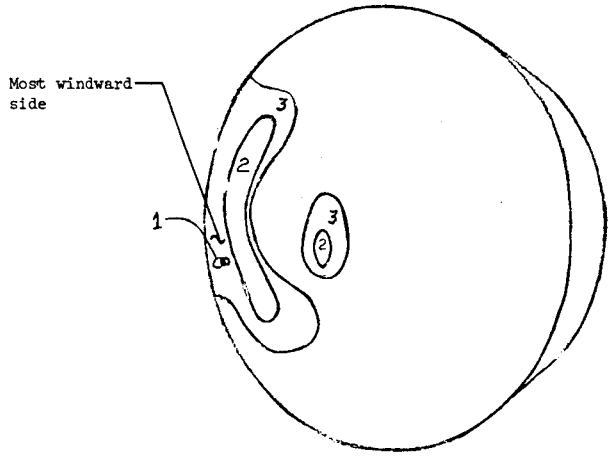

R/M= 1.71049E+07
HS= 4.88652E+02

CONTOUR	T,SEC	H/HS
1	2.30	1.37745E+00
2	3.60	1.10100E+00
3	5.00	9.34230E-01

(f) $\alpha = 15^{o}$.

Figure 16.- Continued.

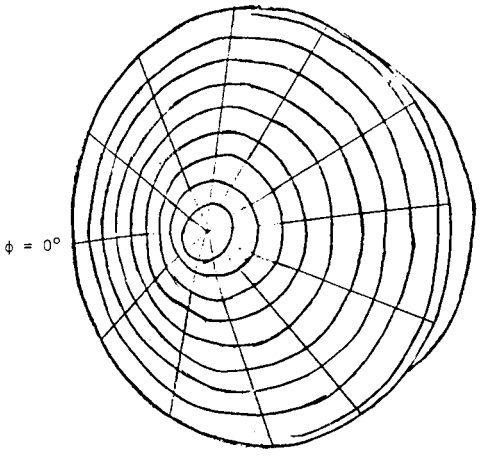

Grid model 2

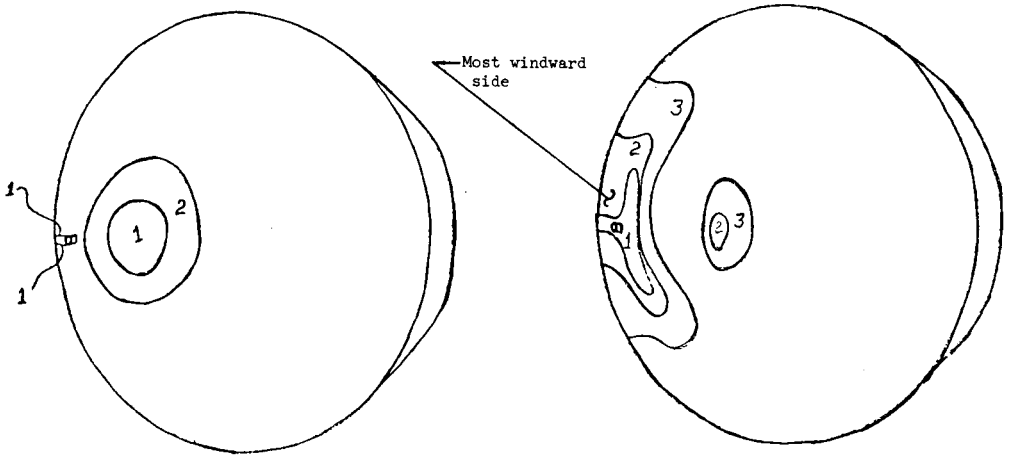

R/M= 3.96834E+06
HS= 2.23191E+02
CONTOUR T,SEC H/HS
1 1.00 5.54912E-01
2 1.60 7.11749E-01

R/M= 1.60632E+07
HS= 4.84956E+02
CONTOUR T,SEC H/HS
1 2.60 1.16569E+00
2 3.40 1.05784E+00
3 5.10 8.63726E-01

(g) $\alpha = 18^{\circ}$.

Figure 16.- Concluded.

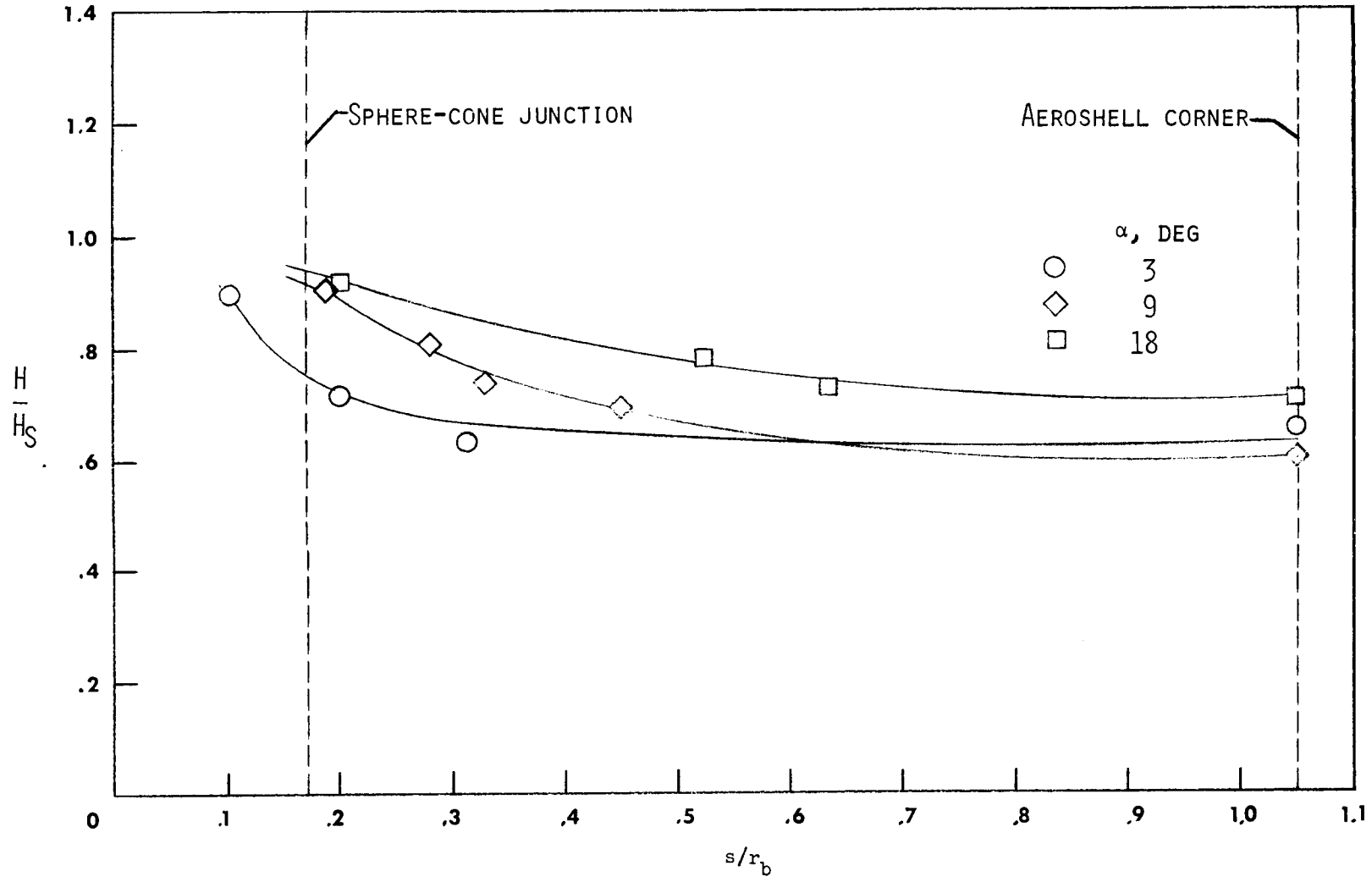

(a) Model 1.

Figure 17.- Effect of angle of attack on the windward-ray heat-transfer coefficients at a Reynolds number per meter of 3.7×10^6.

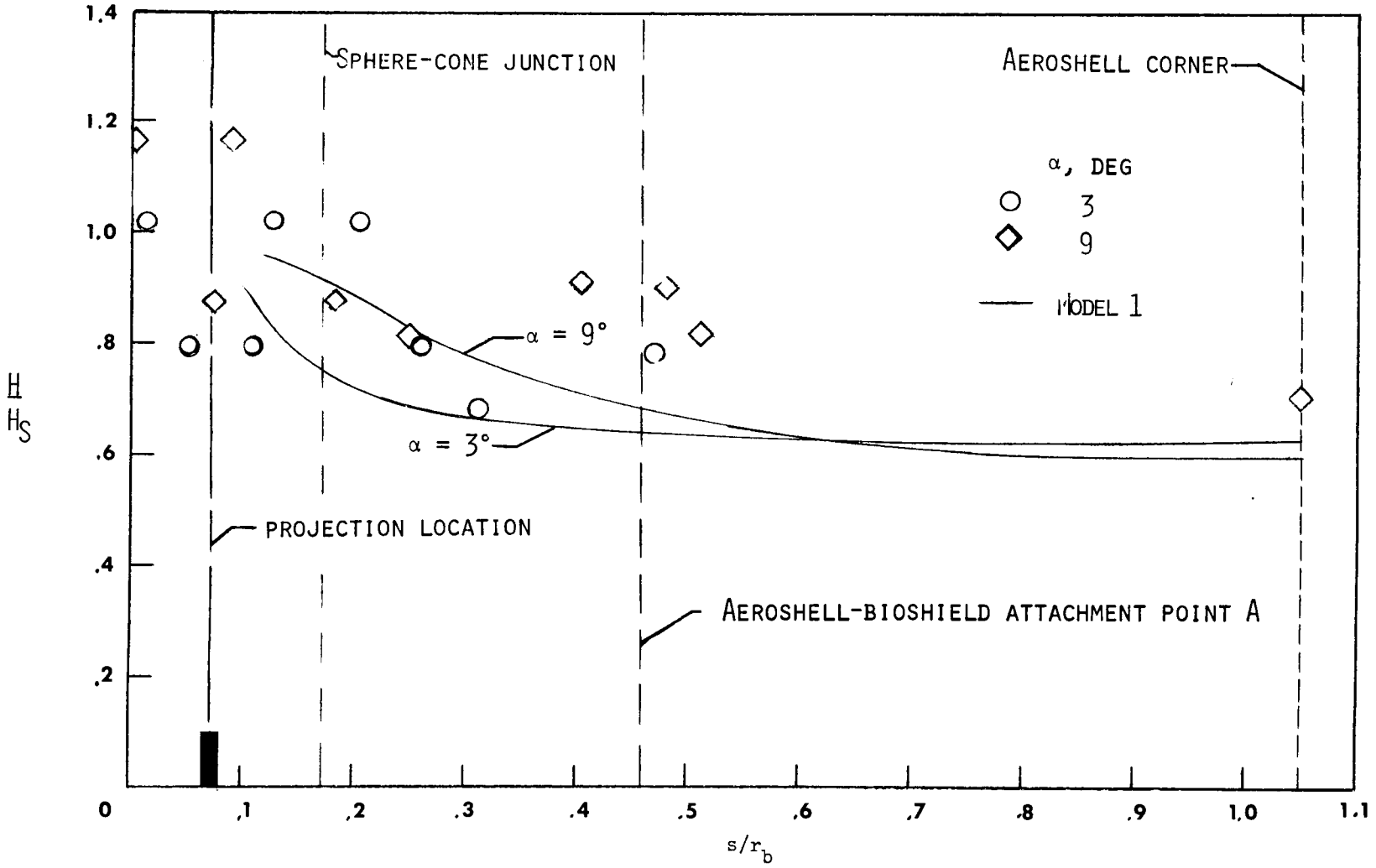

(b) Model 2.

Figure 17.- Continued.

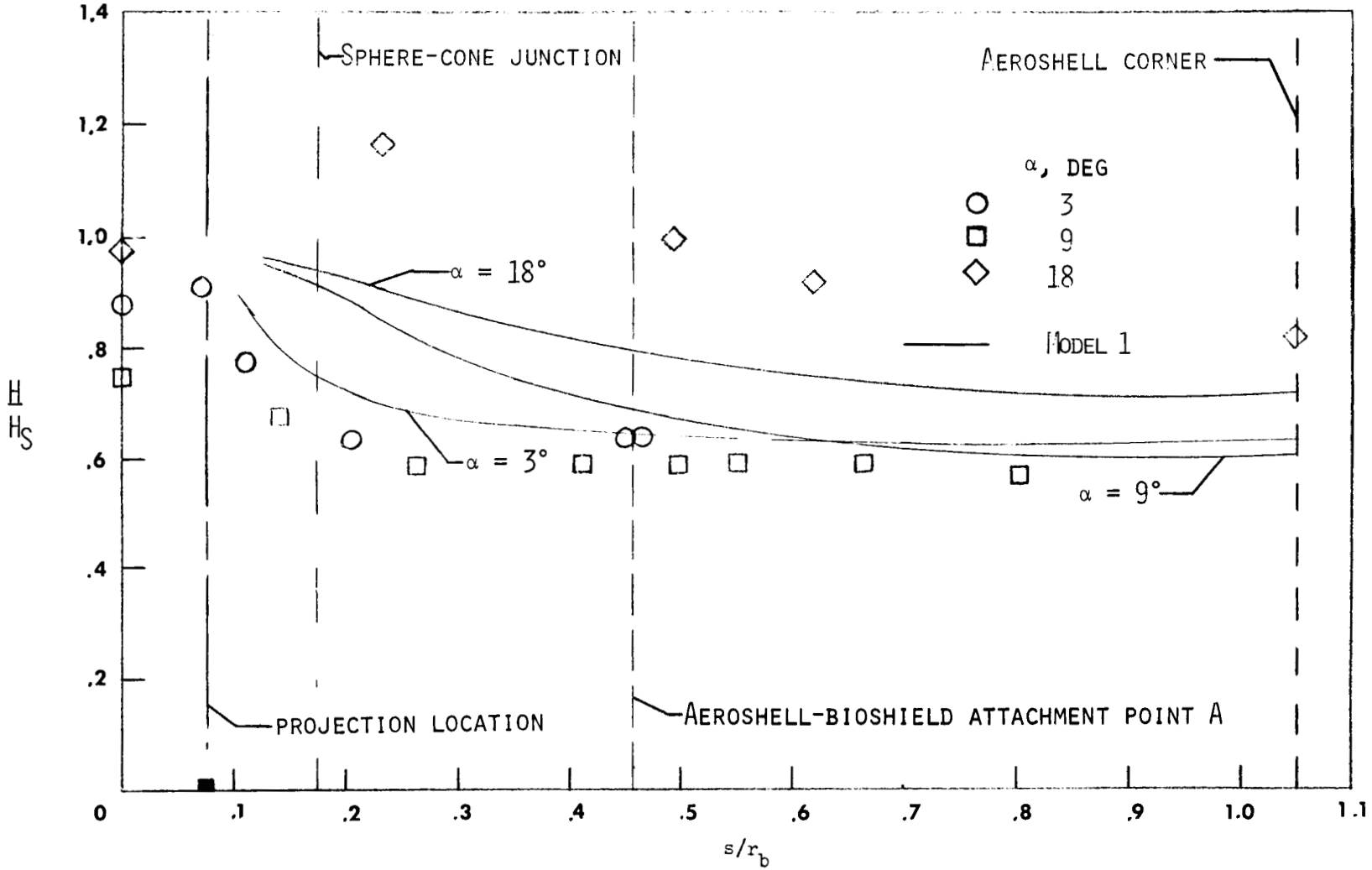

(c) Model 3.

Figure 17.- Concluded.

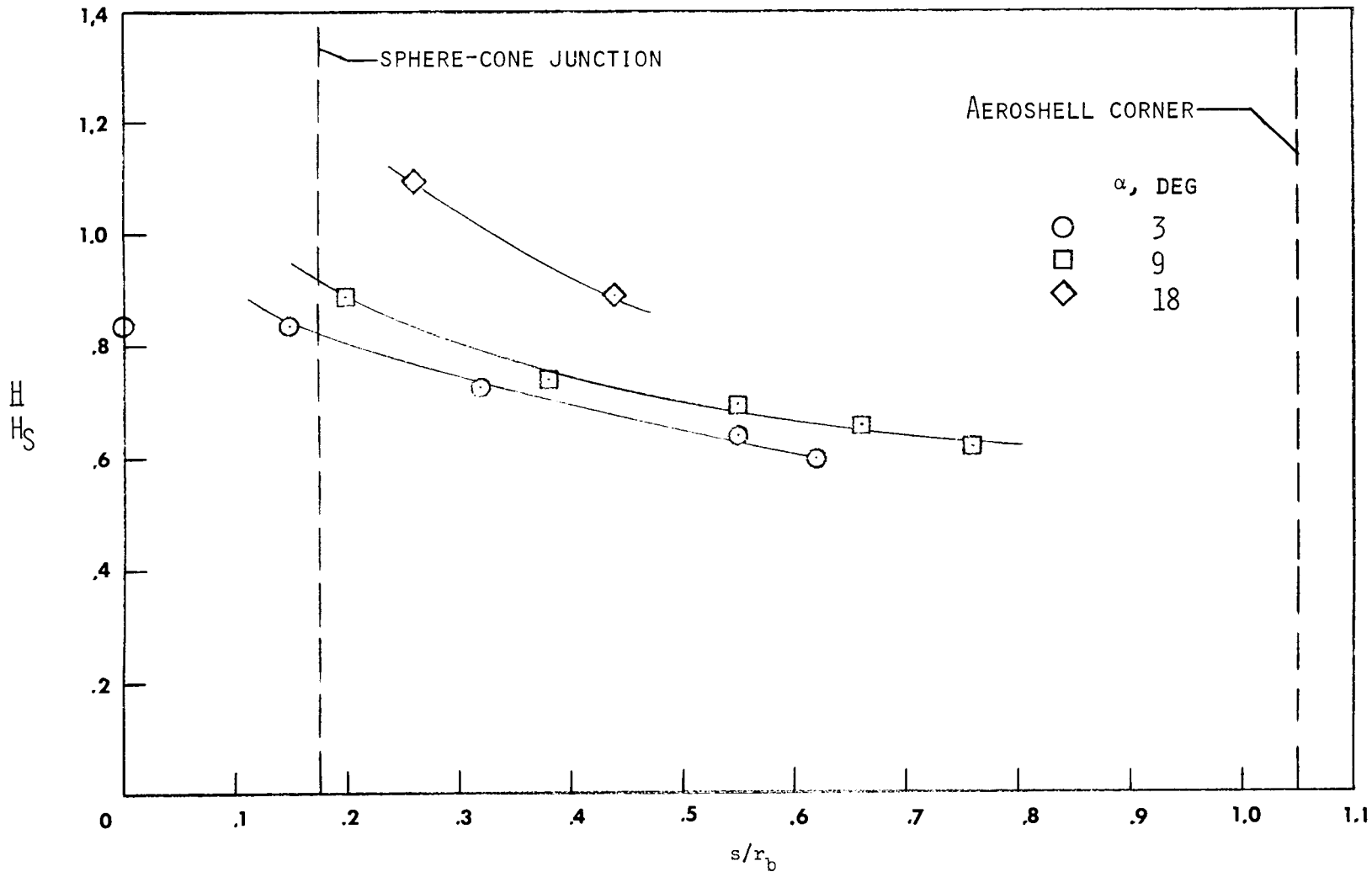

(a) Model 1.

Figure 18.- Effect of angle of attack on the model windward-ray heat-transfer coefficients at a Reynolds number per meter of 17×10^6.

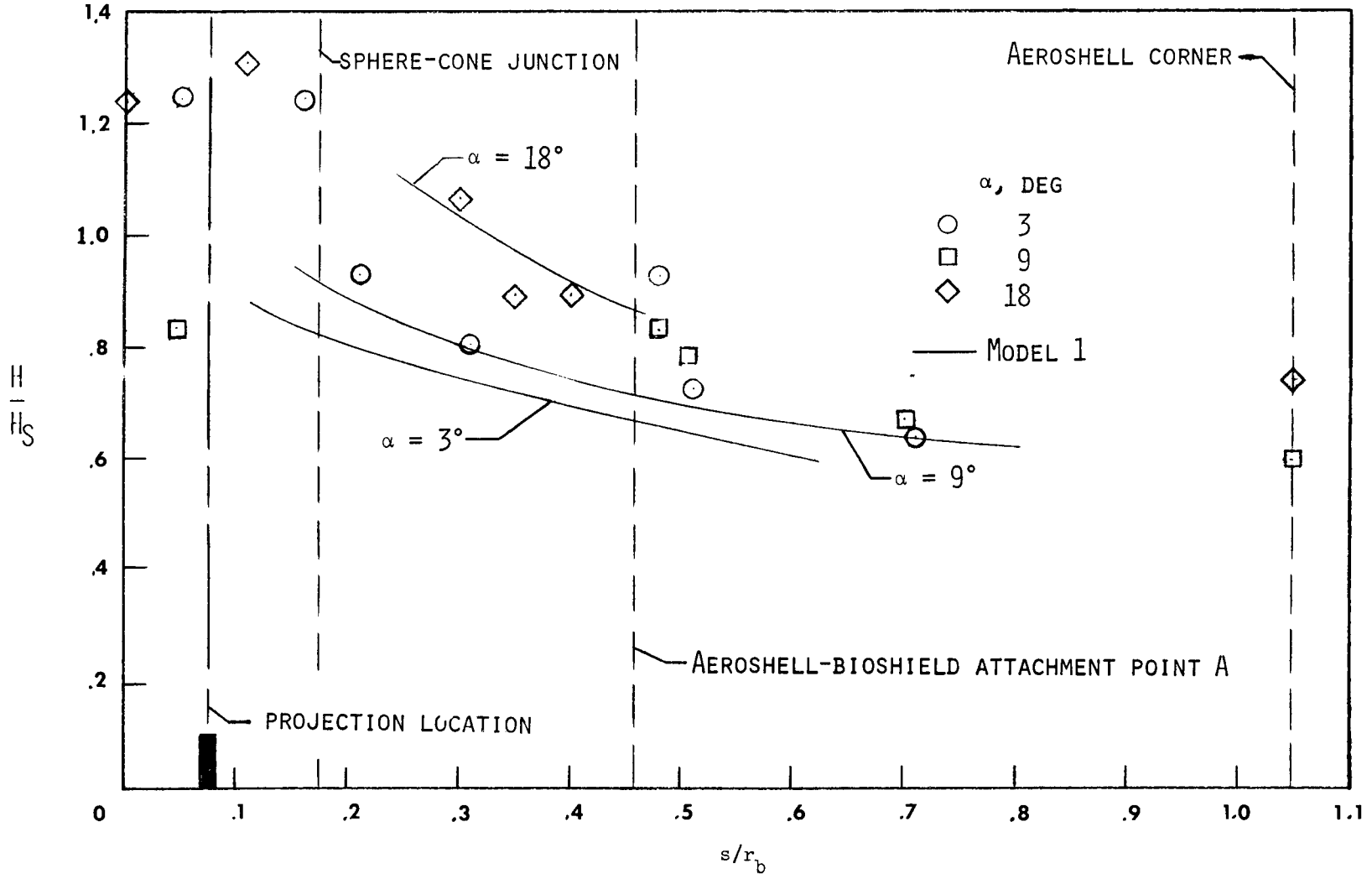

(b) Model 2.

Figure 18.- Continued.

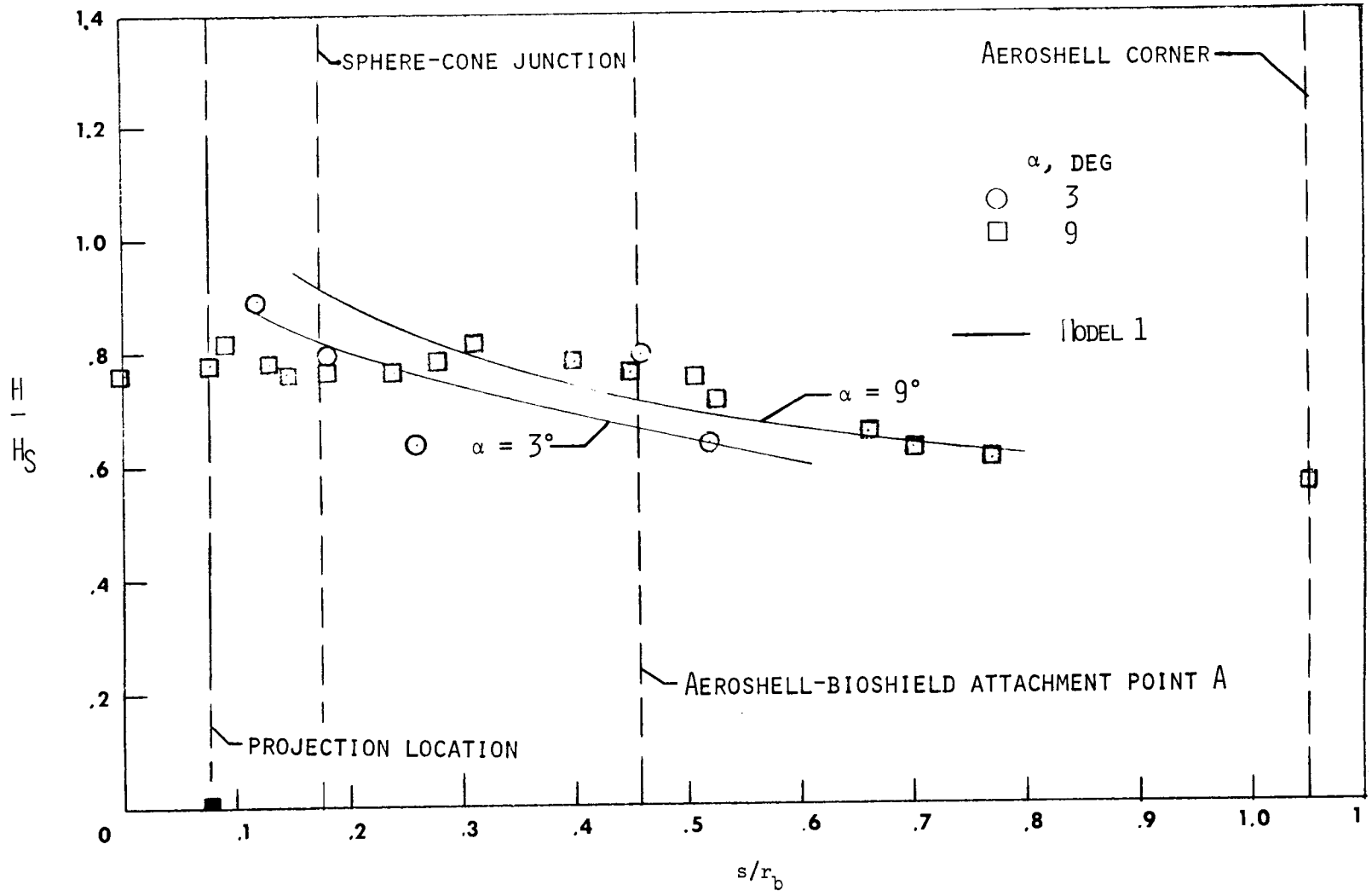

(c) Model 3.

Figure 18.- Concluded.

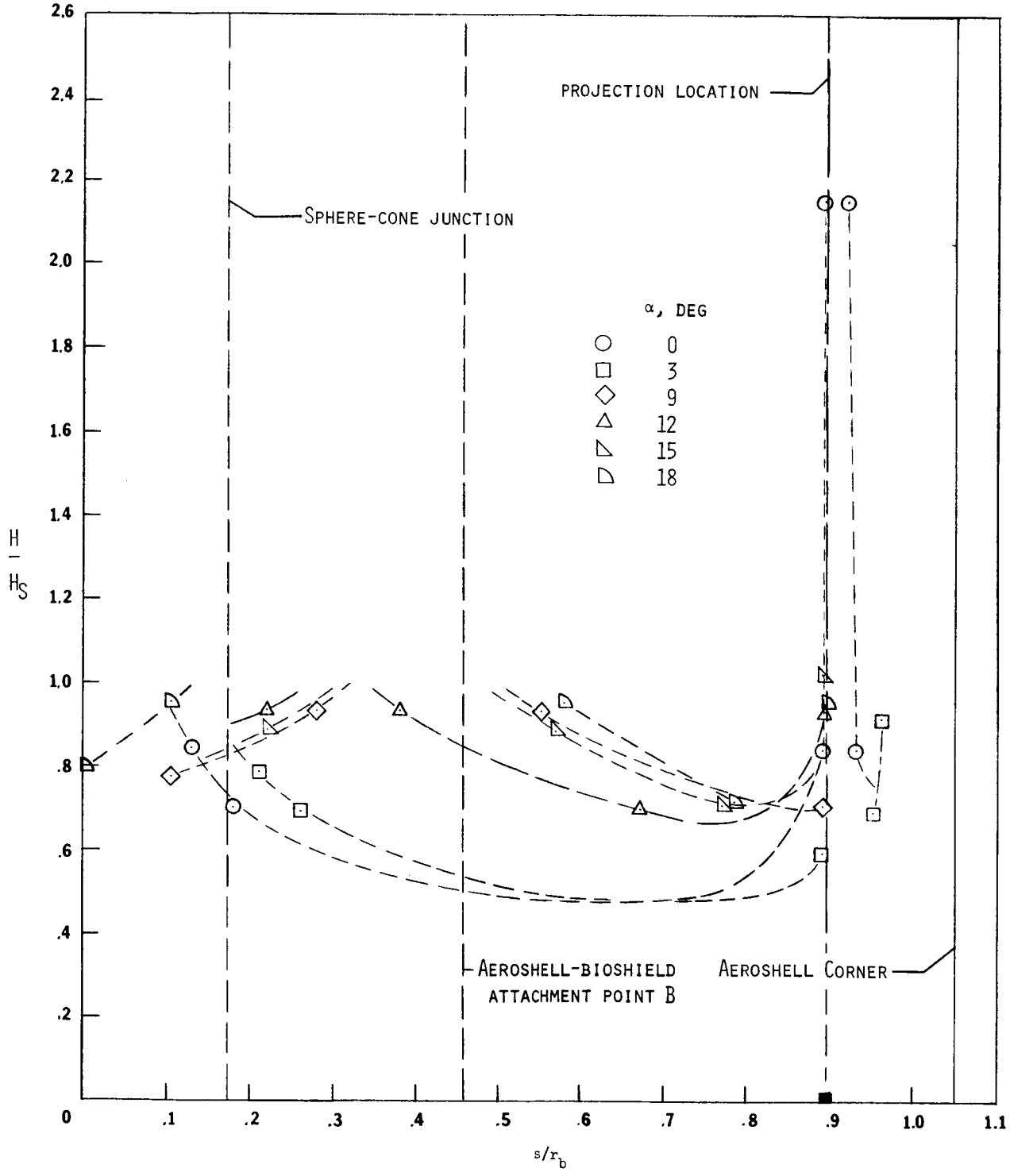

(a) Reynolds number per meter $\approx 3.7 \times 10^6$.

Figure 19.- Heat-transfer-coefficient distribution on the most windward ray of model 5.

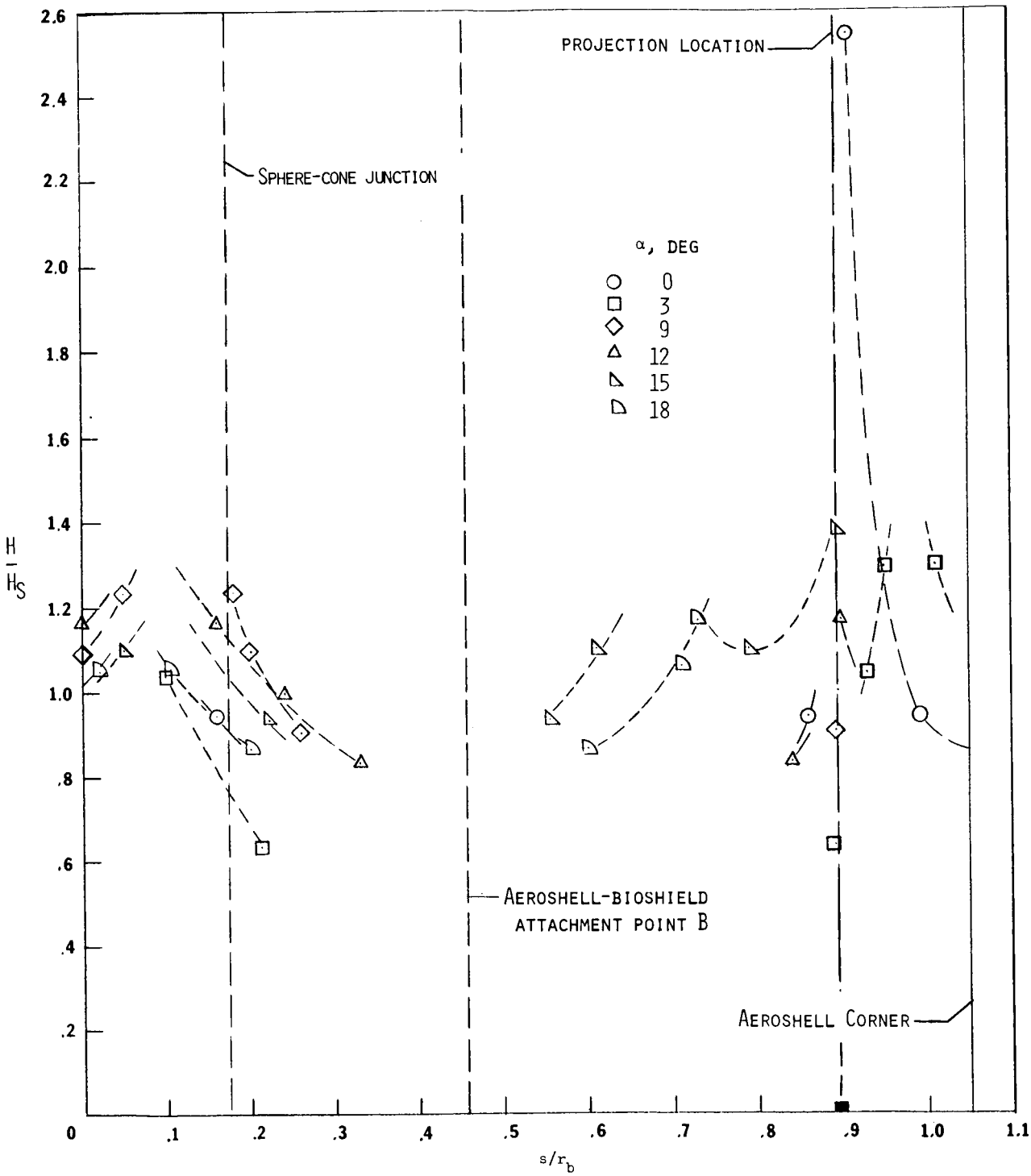

(b) Reynolds number per meter $\approx 17 \times 10^6$.

Figure 19.- Concluded.

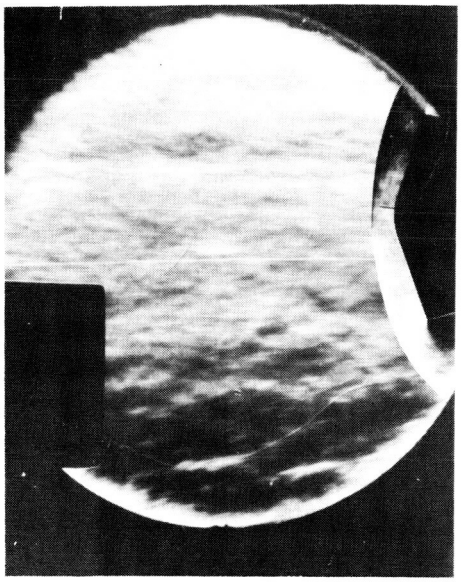

(a) $\alpha = 0^{\circ}$.

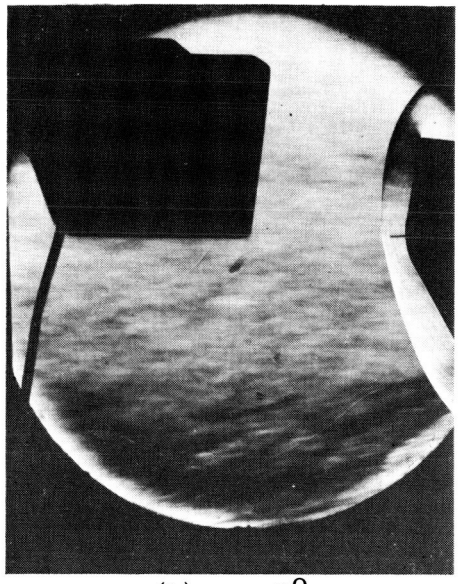

(b) $\alpha = 9^{\circ}$.

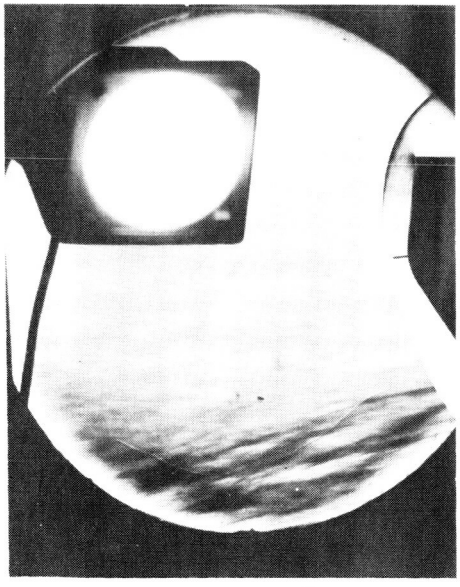

(c) $\alpha = 12^{\circ}$.

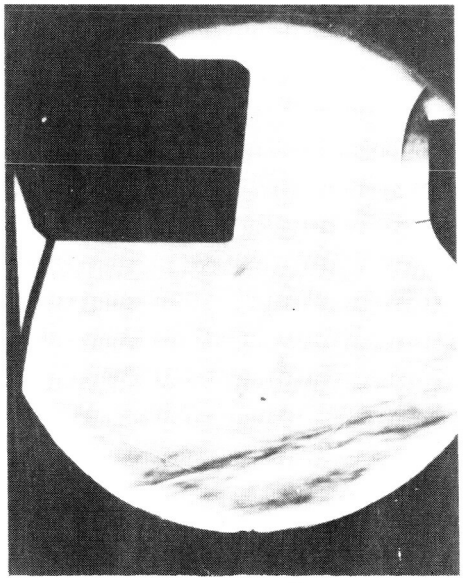

(d) $\alpha = 18^{\circ}$.

L-74-1021

Figure 20.- Typical schlieren photographs of model 2 at a Reynolds number per meter of 17×10^6.